The Arabidopsis hnRNP-Q Protein LIF2 and the PRC1 subunit LHP1 function in concert to regulate the transcription of stress-responsive genes

Anne M. Molitor, David Latrasse, Matthias Zytnicki, Philippe P. Andrey, Nicole Houba Hérin, Mélanie Hachet, Christophe Battail, Stefania del Prete, Adriana A. Alberti, Hadi Quesneville, et al.

Plant Cell Advance Publication. Published on August 5, 2016, doi:10.1105/tpc.16.00244

The Arabidopsis hnRNP-Q Protein LIF2 and the PRC1 subunit LHP1 function in concert to regulate the transcription of stress-responsive genes

Short title

LIF2 and LHP1 target a common set of stress genes

Anne M. Molitor[a*], David Latrasse[a*], Matthias Zytnicki[b*], Philippe Andrey[a,c], Nicole Houba-Hérin[a], Mélanie Hachet[b], Christophe Battail[d], Stefania Del Prete[a,] Adriana Alberti[e], Hadi Quesneville[b], Valérie Gaudin[a,1]

[a] Institut Jean-Pierre Bourgin, INRA, AgroParisTech, CNRS, Université Paris-Saclay, F-78000 Versailles, France

[b] URGI, INRA, Université Paris-Saclay, F-78000 Versailles, France

[c] Sorbonne Universités, UPMC Université Paris 06, UFR927, F-75005, Paris, France

[d] CEA-Institut de Génomique-Centre National de Séquençage, F-91057 Evry, France

[e] CEA-Institut de Génomique, Genoscope, Centre National de Séquençage, F-91057 Evry, France

* Equally contributed

1 Corresponding author: Valérie Gaudin

Institut Jean-Pierre Bourgin, INRA, AgroParisTech, CNRS, Université Paris-Saclay, INRA Centre de Versailles-Grignon, RD10 Route de Saint-Cyr, F-78026 Versailles, France

E-mail: valerie.gaudin@versailles.inra.fr - Tel +33 1 30 83 35 22

The author responsible for distribution of materials integral to the findings presented in this article in accordance with the policy described in the Instructions for Authors (www.plantcell.org) is: Valérie Gaudin (valerie.gaudin@versailles.inra.fr)

Synopsis

ChIP-seq analyses of the RBP LIF2 and its LHP1 partner in various backgrounds and stress conditions revealed target regions for the two proteins enriched in antagonistic marks.

Abstract

LHP1-INTERACTING FACTOR2 (LIF2), a heterogeneous nuclear ribonucleoprotein involved in *Arabidopsis thaliana* cell fate and stress responses, interacts with LIKE HETEROCHROMATIN PROTEIN1 (LHP1), a Polycomb Repressive Complex1 (PRC1) subunit. To investigate LIF2-LHP1 functional interplay, we mapped their genome-wide distributions in wild-type, *lif2,* and *lhp1* backgrounds, under standard and stress conditions. Interestingly, LHP1-targeted regions form local clusters, suggesting an underlying functional organization of the plant genome. Regions targeted by both LIF2 and LHP1 were enriched in stress-responsive genes, the H2A.Z histone variant, and antagonistic histone marks. We identified specific motifs within the targeted regions, including a G-box-like motif, a GAGA motif, and a *telo*-box. LIF2 and LHP1 can operate both antagonistically and synergistically. In response to methyl jasmonate treatment, LIF2 was rapidly recruited to chromatin, where it mediated transcriptional gene activation. Thus, LIF2 and LHP1 participate in transcriptional switches in stress-response pathways.

Introduction

In eukaryotes, the control of gene expression is central to development and environmental adaptation. The establishment and maintenance of specific transcriptionally active and repressive chromatin states participate in this control. Polycomb Repressive Complexes (PRCs) and Trithorax (Trx) Complexes shape chromatin states and have general transcriptional repressor and activator activities, respectively (Simon and Kingston, 2013; Del Prete et al., 2015). Over the past few years, the regulatory function of PRCs has been challenged in both plants and animals (Tavares et al., 2012; Simon and Kingston, 2013; Calonje, 2014; Pu and Sung, 2015; Forderer et al., 2016). For instance, novel PRC1 complexes have been identified; the canonical model of PRC repression, in which PCR2-dependent H3K27 trimethylation is followed by PRC1-dependent H2A monoubiquitination, is no longer regarded as the unique mode of action (Tavares et al., 2012; Calonje, 2014); and a novel transcriptional activation function has been reported for PRC1 (Gil and O'Loghlen, 2014).

However, the mechanism underlying the transition from active to repressed chromatin states remains poorly understood. Documented recruitment of Polycomb group proteins (PcG) to chromatin identified thousands of target regions in eukaryotic

genomes. In plants, the PRC1 subunit LHP1 is distributed throughout the genome and co-localizes with the H3K27me3 repressive histone mark (Turck et al., 2007; Zhang et al., 2007), as observed for animal PcG proteins. The distribution of FERTILIZATION INDEPENDENT ENDOSPERM (FIE), a plant PRC2 subunit, somewhat overlaps with H3K27me3 regions (Deng et al., 2013). The chromatin context, which is determined by the combination of specific DNA motifs, histone marks, or other chromatin-associated proteins, largely determines PcG recruitment. For instance, *Drosophila* PRCs contain sequence-specific DNA-binding factors and are classically recruited at Polycomb/Trithorax Response Elements (PRE/TREs or PREs) in the genome, which are composed of a variable combination of short DNA motifs and participate in the maintenance of the transcriptional status (Bauer et al., 2015). Only a few PRE-like elements have been reported in mammals (Bauer et al., 2015). PRCs interact with various chromatin-associated proteins, such as histone modifying enzymes or transcription factors (TFs), which may also contribute to their targeting. In plants, several TFs, such as SCARECROW, ASYMMETRIC LEAVES 1 (AS1), and AS2, interact with PRC subunits (reviewed in (Del Prete et al., 2015)). Recently, the *A. thaliana* GAGA-binding factor BPC6 was shown to recruit LHP1 to GAGA motifs (Hecker et al., 2015), reminiscent of the recruitment of PcG proteins to GAGA motifs present in animal PREs. Finally, whereas some long non-coding RNAs (lncRNAs) are involved in the scaffolding of chromatin modifying complexes associated with PRC function (Brockdorff, 2013) or mediate intrachromosomal interactions (Zhang et al., 2014), they also emerged as novel interacting partners of both PRC2 and PRC1 subunits (Del Prete et al., 2015) that participate in their genomic recruitment. In *A. thaliana*, lncRNAs were proposed to function in the transcriptional regulation of *FLOWERING LOCUS C* (*FLC)* mediated by PcG proteins (Swiezewski et al., 2009; Heo and Sung, 2011; Csorba et al., 2014). Intriguingly, LIF2, a heterogeneous nuclear ribonucleoprotein Q (hnRNP-Q) with three RNA recognition motifs (RRMs), was identified as a partner of LHP1 (Latrasse et al., 2011), highlighting the diversity of plant proteins associated with PRC1, and suggesting that RNA-binding proteins (RBPs) mediate interactions between plant PRC1 and RNA components.

To investigate the interplay between LIF2 and LHP1, we compared the genome-wide chromatin profiles of LIF2 and LHP1 in wild-type and mutant backgrounds. This is the first report of the genome-wide chromatin profile of a plant RBP. Our ChIP-seq data analyses revealed that LIF2 had a more restricted distribution than LHP1, being

mainly present at stress-responsive genes. The spatial analysis of LHP1 distribution showed that LHP1 regions tend to aggregate locally, suggesting a role for LHP1 in genome topography. Specific and antagonistic histone marks were associated with each protein, as well as *cis*-regulatory DNA elements. We identified the GAGA motif and *telo*-box motifs in the LHP1 target genes. Also present in FIE binding sites (Deng et al., 2013), these two motifs may thus be part of a PRC targeting signature. Given the role of LIF2 in pathogen responses (Le Roux et al., 2014), we investigated the distribution of LIF2 in response to methyl jasmonate (MeJA), a key hormone in plant biotic and abiotic stress responses. We showed that LIF2 distribution was dynamic in response to MeJA treatment and that LIF2 was required for transcriptional gene activation. Thus, we highlighted a complex interplay between LIF2 and LHP1 in stress-response pathways.

Results

LIF2 and LHP1 target a common set of chromatin regions

Prompted by the observation that hnRNP-Q LIF2 physically interacts with the chromatin-associated protein LHP1 (Latrasse et al., 2011), we performed ChIP-seq experiments to identify the chromatin regions enriched in LIF2 and LHP1 (enrichment regions, ERs). For this purpose, we produced transgenic lines expressing 3xHA-tagged LIF2 (HA:LIF2) and 3xHA-tagged LHP1 (LHP1:HA) under the control of endogenous genomic regulatory sequences, in the *lif2-1* and *lhp1-4* genetic backgrounds, respectively. Two independent ChIP-seq libraries were sequenced for each protein (Figure 1). We observed good overlaps between replicates, as well as high Pearson coefficients of the MACS peak fold-change correlations between replicates (0.93 (LIF2) and 0.81 (LHP1); Supplemental Figure 1). We identified 1457 ERs present in both replicates for LIF2 and 4844 for LHP1 (at a false discovery rate (FDR) of < 0.05), and determined the summit (i.e., position with the maximum read number) in each ER. The comparison of the two genome-wide distributions allowed us to identify 488 genomic regions where LIF2 and LHP1 were detected, corresponding to the intersection of the two genomic distributions (named LIF2-LHP1 IRs, intersect regions) (Figures 1 A and 1 B). We confirmed binding to ten ERs by ChIP experiments followed by quantitative PCR (ChIP-qPCR) (Supplemental Figure 1). We established that 52.8% of the DamID-identified LHP1 target genes (Zhang et al., 2007) were present in our ChIP-seq data set (despite differences in tissue, developmental stages, and growth conditions). These data suggest that LIF2 has a more specialized function in the genome than does LHP1, with each protein having independent and specific functions. However, in agreement with their physical interactions, a subset of genomic regions was identified where the two proteins were located.

LIF2 is present in narrow chromatin regions in 5’ and 3’ UTRs

LIF2 and LHP1 exhibited different chromatin-associated profiles. Whereas the LIF2 profile had narrow, discrete peaks, LHP1 peak sizes were larger (Figure 1 C). By analyzing the distribution of LIF2 and LHP1 over annotated genomic features and comparing this distribution with a random distribution over genome regions of similar size, we found that LIF2 had a preference for 5' UTRs (2.52-fold compared to LIF2-random), exons (especially exon 1) (Supplemental Figure 2), and 3' UTRs (4-fold

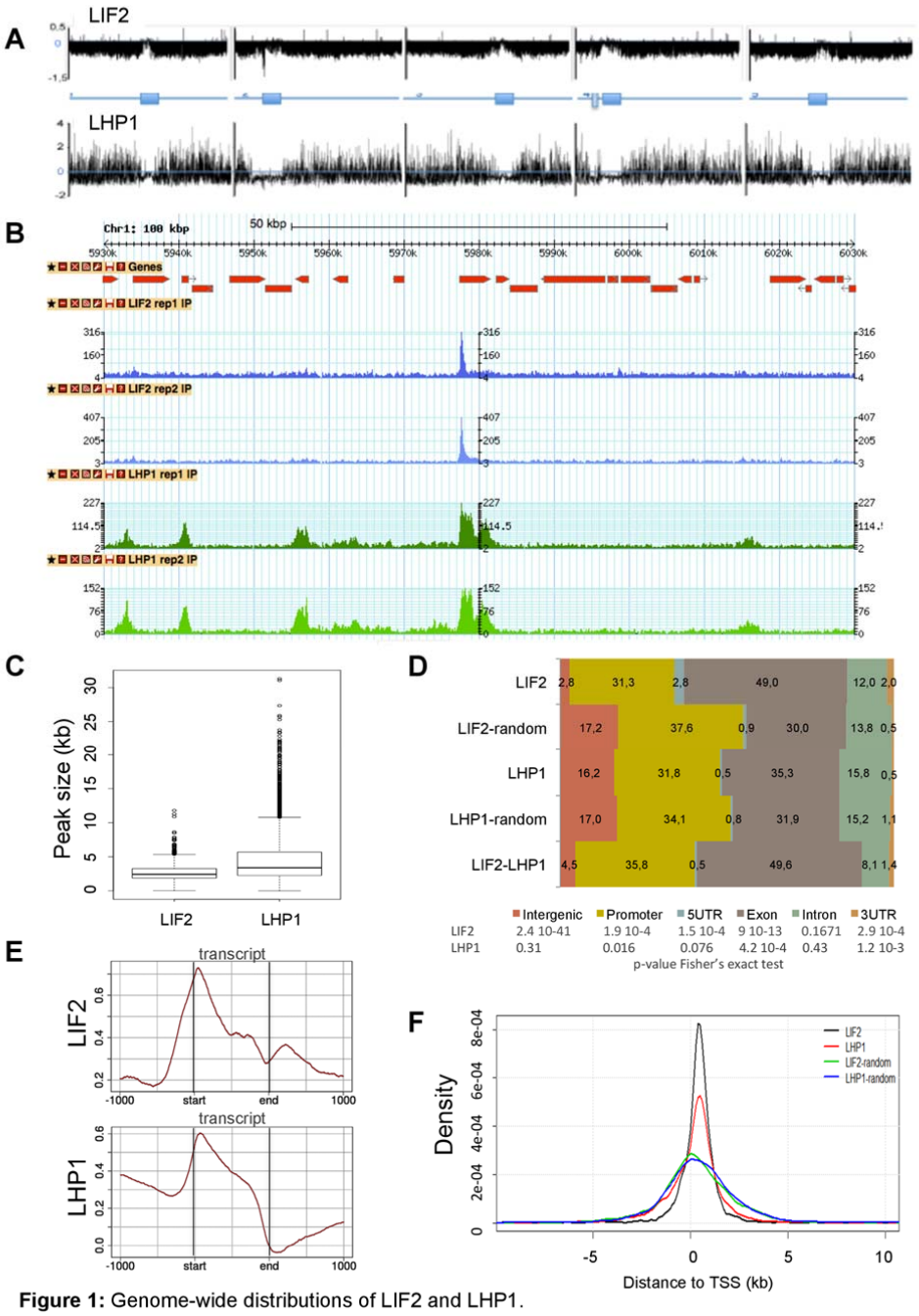

Figure 1: Genome-wide distributions of LIF2 and LHP1.
(**A**) Chromosomal view of the peaks using model-based analysis.
(**B**) Screenshot of a 100-kb window with the distributions.
(**C**) Size distributions of the ERs defined as intersects of MACS peaks for the biological replicates.
(**D**) Distributions of ER-associated annotations (percentage). Regions with identical sizes were randomly shuffled in the genome and compared with the observed ERs, using a Fisher's exact test.
(**E**) Distributions of IP enrichment (log2(# reads IP/ # read input)) over the transcript structures.
(**F**) Distance to closest transcriptional start sites (TSS) of LIF2 and LHP1 ERs, and the corresponding randomized regions.

and the PRC1 subunit LHP1 function in concert to regulate the transcription of

compared to LIF2-random), whereas LHP1 had a more balanced distribution over all regions (Figure 1 D). Interestingly, the distribution of the LIF2-LHP1 IRs was similar to that of the LIF2 ERs. Our analysis of the peak distributions over transcripts showed that LIF2 was enriched at transcription start sites (TSSs) and depleted at transcription termination sites (TTSs) (Figure 1 E). The low but significant level of LIF2 downstream TTSs was not due to the proximity of another TSS. LHP1 was more prevalent at promoter regions and gene bodies, with a marked preference for TSSs, resulting in an asymmetry between upstream and downstream genic regions (Figure 1 E). The presence of LIF2 and LHP1 ERs in regions close to the TSS was confirmed with the analysis of the distance of the ERs to the closest TSS compared to the randomly shuffled control regions (Figure 1 F).

The targeted regions tend to form clusters

Given the role of PcG proteins in structuring the genome in animal species (Del Prete et al., 2015), we analyzed the distribution of LHP1 and LIF2 along each chromosome. The distribution of the number of ER summits in 1-Mb windows revealed that portions of the genome were enriched for LHP1 and LIF2 (Figure 2 A, Supplemental Figure 3). To analyze the distribution of LHP1 ERs further and to test the existence of an underlying organization principle in this distribution, we compared the summit distribution of LHP1 ERs to a random distribution model, conditioned on the size of LHP1 ER regions. Observed and model-predicted distributions were compared using local-scale (i.e., cumulative distribution of the distance between each ER and its closest neighbor) and global-scale (i.e., cumulative distribution of the inter-distances between all ERs) spatial descriptors. A significant discrepancy with the completely random model was observed at the local scale, with the measured distances between ERs and their closest neighbors being significantly smaller than expected under a random distribution for all chromosome arms (Figure 2 B, Supplemental Figure 4). Compared to the random distribution, the distance to the closest ER was enriched in the range of short values of up to ~10 kb (Figure 2 C). This range was constant across chromosome arms, suggesting the existence of common spatial constraints despite differences in arm length and ER density. Overall, no significant difference to the random distribution was observed (Figure 2 D, Supplemental Figure 5) when comparing the distribution of all inter-distances (Figure 2 D, Supplemental Figure 4), consistent with the globally uniform distribution of LHP1 ERs in 1-Mb windows (Figure 2 A, Supplemental Figure 3). LIF2 ERs

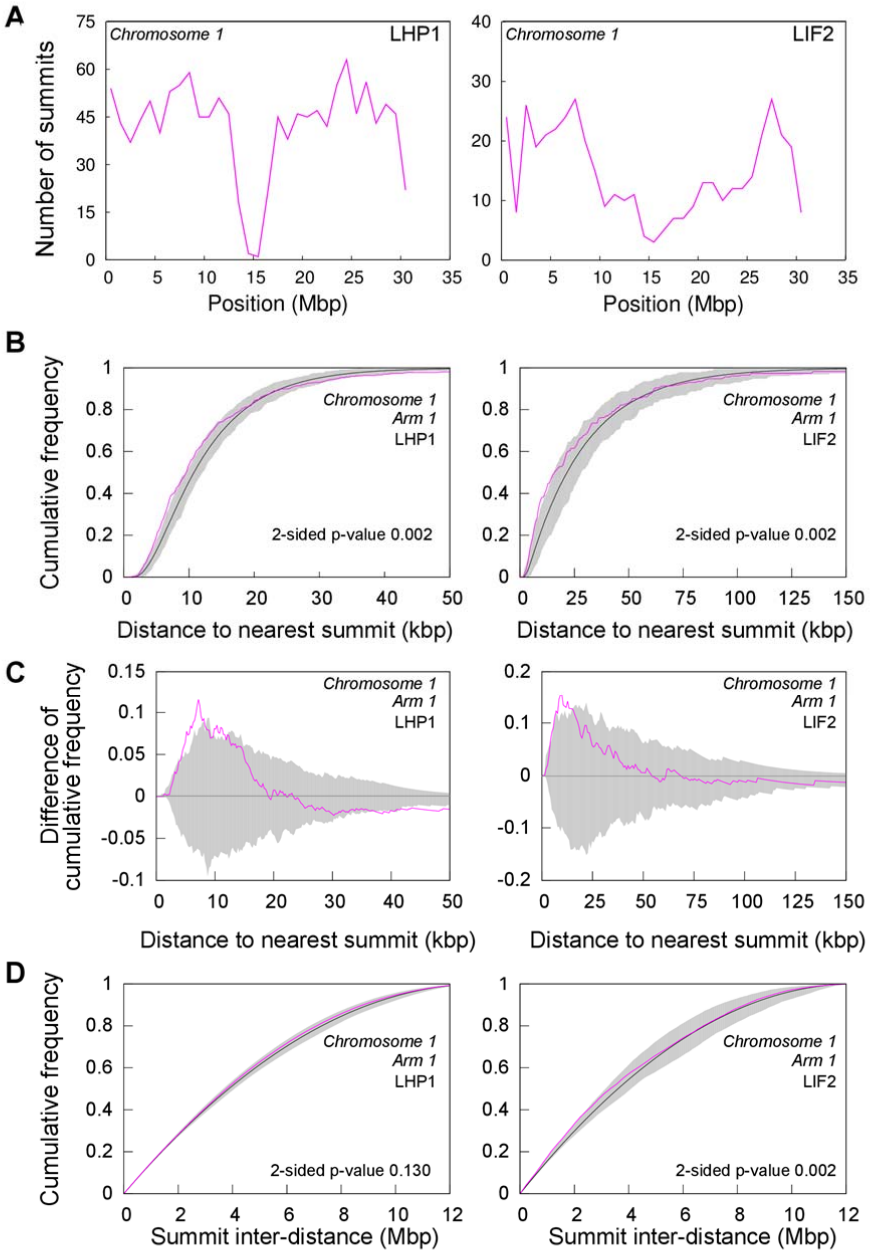

Figure 2: Non-random distributions of the LHP1 ERs and LIF2 ERs in the *A. thaliana* genome.
(**A**) Number of summits in 1-Mb windows along Chromosome 1.
(**B-D**) Observed (pink) and random model (black: average; grey: 95% envelope) distributions of distance to nearest ER (B-C) and of all ER inter-distances (D), on the first arm of Chromosome 1. Similar results were obtained for all chromosome arms (Supplemental Figures 2, 3 and 4).

exhibited spatial clustering that was similar to that of LHP1 ERs. Despite the lower density of LIF2 ERs, the range of distances between nearest neighbors was similar to that observed for LHP1 ERs (Figure 2 C), suggesting that the distributions of the two proteins' target regions were under shared constraints.

To further investigate the clustering of LHP1 ERs, we analyzed the relationship between the LHP1 ER genome-wide distribution and the distribution of repeated genes in the *A. thaliana* genome. Indeed, repeated genes may participate in this clustering tendency. It was previously shown using ChIP-chip experiments that out of the 679 tandemly repeated genes located on chromosome 4, 30% were targeted by LHP1 (Turck et al., 2007). In the whole *A. thaliana* genome, 1564 tandem duplications (T-clusters) and 1680 segmental duplications (with a 1:1 duplication relation, S-clusters) were described (Haberer et al., 2004). The T-clusters contain from 2 to up to 21 repeated genes, with a mean value <3 genes. Using our ChIP-seq data, we observed that 20.6% of the T-cluster genes were targeted by LHP1, compared to 11.7% for the S-cluster genes. However, only 23.1% of the LHP1-targeted genes were located in T-clusters. On average, there was less than one LHP1 target gene per T-cluster and only 11% of T-clusters had two or more LHP1 target genes, accounting for only 9.6% of all LHP1 targets (Supplemental Table 1). These low figures suggest that LHP1 binding to T-cluster genes is not sufficient to explain the clustering tendency of LHP1-targeted regions observed at the local scale on the chromosome arms.

The presence of antagonistic histone marks and H2A.Z characterize LIF2-LHP1 IRs

A limited number of chromatin states, which are based on histone post-translational modifications (PTMs) or histone variants, have been reported for the *A. thaliana* genome (Sequeira-Mendes et al., 2014). We thus examined whether specific epigenetic marks were preferentially associated with the identified ERs, using data sets for nine histone marks (Luo et al., 2012) and the H2A.Z histone variant (Zilberman et al., 2008; Coleman-Derr and Zilberman, 2012). We observed that LHP1 ERs were enriched in the repressive mark H3K27me3, confirming our previous genome-wide analysis (Zhang et al., 2007), and were depleted in active histone marks, such as H3K4me3 (Figure 3, Supplemental Figure 6). By contrast, LIF2 ERs were enriched in H3K4me3 and H3K9ac histone marks, which are hallmarks of active/open chromatin. Interestingly, a similar enrichment in H3K4me3 and H3K27me3 was observed in LIF2-LHP1 IRs, and this was associated with a noticeable depletion in the active mark H3K36me3 compared to LIF2 ERs. LIF2 and LHP1 ERs also had similar levels of H2A.Z, with LIF2-LHP1 IRs having slightly higher levels. In *A. thaliana*, H2A.Z is enriched within the nucleosomes surrounding

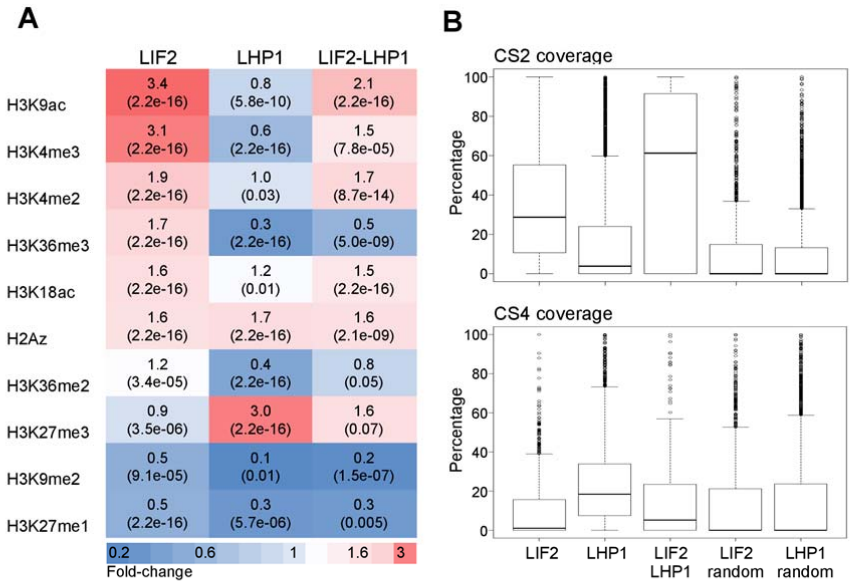

Figure 3. Post-translational histone modifications (PTMs) and the H2A.Z histone variant in the LIF2 ERs, LHP1 ERs or LIF2-LHP1 IRs .
(**A**) Heat map presenting the fold changes (p-value paired t-test) between targeted and randomized regions.
(**B**) Percentage of chromatin states 2 and 4 (CS2 and CS4; defined by Sequeira-Mendes et al., 2014) covering LHP1 ERs, LIF2 ERs, and LIF2-LHP1 IRs, and randomized control regions.

234 the TSSs of genes (Zilberman et al., 2008), but also across the bodies of genes with
235 low transcription levels and high responsiveness (Coleman-Derr and Zilberman,
236 2012). Our data suggest that LIF2-LHP1 IRs may correspond to subdomains of
237 chromatin state 2 (CS2), which is characterized by relatively high levels of both active

H3K4me3 and inactive H3K27me3 histone marks and is mostly associated with bivalent regions and highly constrained gene expression (Sequeira-Mendes et al., 2014). We thus analyzed the coverage of CS2 in the distributions of LHP1 and LIF2 ERs and compared this coverage with CS4 coverage, CS4 having high levels of H3K27me3, but reduced levels of active marks. We confirmed enrichments in CS2 for both LIF2 IRs and LIF2-LHP1 IRs (Figure 3 B). By comparing the lists of LIF2 and LHP1 target genes with the bivalent genes identified by sequential ChIP experiments (Luo et al., 2012), we observed that about 14.92% of the LIF2-LHP1 IR genes have been annotated as bivalent (Luo et al., 2012), whereas only 4.97% and 5.97% of the LIF2 and LHP1 target genes have been annotated as bivalent, respectively. Thus, the genome-wide distributions of LIF2 and LHP1 contributed to the functional topographical organization of the *A. thaliana* genome (Sequeira-Mendes et al., 2014).

LIF2-LHP1 IRs are enriched in stress-responsive genes

To predict the functions of genes of LIF2 ERs and LIF2-LHP1 IRs, we determined the gene responsiveness index of the binding regions based on the expression profiles of the genes located in the ERs (Aceituno et al., 2008; Coleman-Derr and Zilberman, 2012). We found that they were enriched in responsive genes (Figure 4 A). Our analysis of the functional Gene Ontology (GO) terms revealed that LIF2 ERs and LIF2-LHP1 IRs were enriched in stress-responsive genes (Figure 4 A, Supplemental Figures 7 and 8). The Bio-Array Resource for Plant Functional Genomics (BAR) classification Superviewer program (Provart et al., 2003) showed that both LIF2 ERs and LIF2-LHP1 IRs were enriched in the GO term “response to abiotic or biotic stimulus” (normed frequency (NF); LIF2 NF=3, p-value 1.399 10^{-78}; LIF2-LHP1 NF=2.7, p-value 2.662 10^{-19}) (Supplemental Table 2). A more detailed analysis using AgriGO revealed that the first two enriched GO terms for LIF2 ERs were “aromatic compound catabolic process” (NF=29.35, FDR 9.4 10^{-5}, p-value 3.8 10^{-6}) and “callose deposition in cell wall during defense response” (NF=16.57, FDR 1.2 10^{-4}, p-value 5.1 10^{-6}). For LIF2-LHP1 IRs, they were “response to chitin” (NF=4.98, FDR 5.9 10^{-12}, p-value 1.7 10^{-14}) and “regulation of defense response” (NF=3.56, FDR 1.3 10^{-3}, p-value 9.5 10^{-5}) (Supplemental Figure 7). These results were in agreement with those of our previous transcriptome analysis of the *lif2* mutant (Latrasse et al., 2011) and the response of *lif2* to pathogens (Le Roux et al., 2014), but also with the epigenetic marks present at LIF2-LHP1 IRs. Indeed, genes present in CS2 were shown to have constrained transcription profiles (Sequeira-Mendes et al., 2014).

A

Regions	Gene Responsiveness	Ratio
LHP1	23.52	1.099
LIF2	26.63	1.244
LIF2-LHP1	27.42	1.281
Mean value for the genome	21.40	1

B

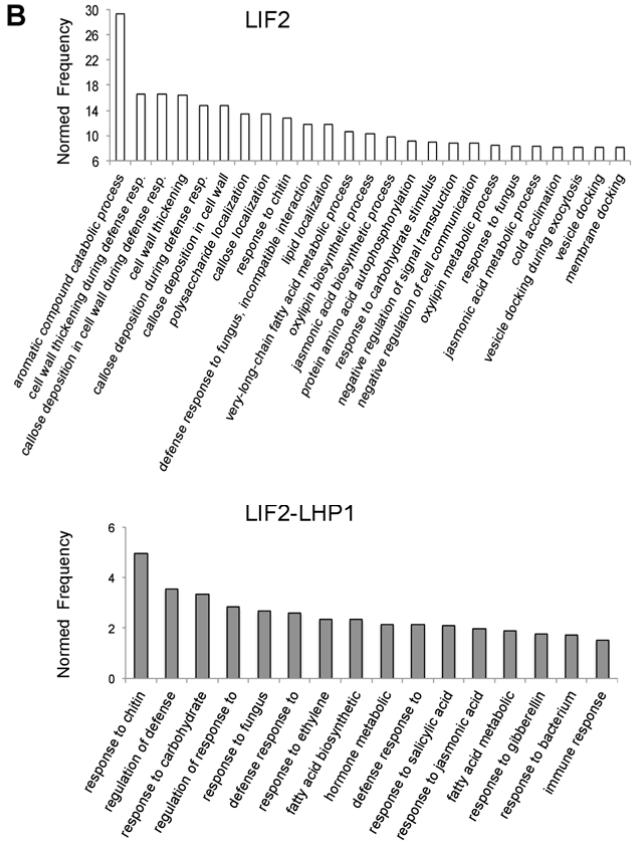

Figure 4: LIF2 binds preferentially stress-response genes.
(**A**) Average gene responsiveness scores were calculated based on a published data set[25] and normalized to the genome-wide average.
(**B**) GO analysis of LIF2 ERs and LIF2-LHP1 IRs using the AgriGO toolkit. The biological process GO terms, with the 25 best normed frequencies (NF) and with NF≥1.5 are presented for LIF2 Ers and LIF2-LHP1 IRs, respectively.

Further GO term analysis revealed an enrichment in “transcription factor activity” in the LIF2 ER and LIF2-LHP1 IR datasets (NF=2.39, p-value 3.730 10^{-18} and NF=3.7, p-value 2.739 10^{-17}, respectively) (Supplemental Table 2). Using the Plant GeneSet Enrichment Analysis (PlantGSEA) (Yi et al., 2013) and Arabidopsis Gene Regulatory

Information Server (AGRIS) (Yilmaz et al., 2011) toolkits, we observed that the main TFs targeted by LIF2 belonged to the AP2-EREBP and WRKY families, consistent with a role for LIF2 in the stress response, whereas TFs in LHP1-ERs belonged to a larger range of families (Supplemental Table 3). Interestingly, TFs present in the 488 LIF2-LHP1 IRs also belonged to the AP2-EREBP family. Some of the target genes were also targeted by other TFs, such as LONG HYPOCOTYL 5 (HY5) (Lee et al., 2007; Zhang et al., 2011) and PHYTOCHROME-INTERACTING FACTOR1 (PIF1) (Chen et al., 2013) (Supplemental Table 4), suggesting a complex interplay between LIF2, LHP1, and TFs.

Identification of *cis*-regulatory DNA elements associated with LIF2 and LHP1 binding

We next searched for putative DNA-binding motifs around the summits. Using the MEME algorithm (Bailey and Elkan, 1995), two consensus motifs were discovered in the 51-bp regions centered on the LIF2-binding summits: a GAGA-like motif and a (C/G)ACGTG(G/T)C(A/G) consensus motif, which belongs to the ACGT-containing element (ACE) family (Figure 5). The ACGTGGCA word was present at moderate levels in the whole genome, mostly in the distal promoter regions of genes (region from -1000 bp to -3000 bp relative to the TSS) (Supplemental Table 5). Some of the ACE elements are recognized by TFs, among which HY5 and PIF1 (Song et al., 2008; Chen et al., 2013), previously identified as having common targets with LIF2 (Supplemental Table 4) and two physically interacting TFs involved in plant growth and, in particular, in the crosstalk between light and reactive oxygen species (ROS) signaling. In the LHP1 datasets, we identified a GAGA-like motif as a putative recognition motif (Figure 5). In addition, we identified the (A/G/T)AACCCTA(A/G) motif. Despite being less represented among the LHP1 peaks, this putative and highly significant DNA motif (-log10(E-value) > 20) was discovered with both MEME and “peak-motif” algorithms (Bailey and Elkan, 1995; Thomas-Chollier et al., 2012) (Figure 5 B). This motif contains the AAACCCTA short interstitial telomere motif, also named the *telo*-box, which was originally described in the 5’ regions of genes encoding the translation elongation factor EF1α and ribosomal proteins (Regad et al., 1994; Gaspin et al., 2010). The AAACCCTA word/*telo*-box is mainly present in introns and 5’ UTRs (Supplemental Table 5). Interestingly, the (A/G/T)AACCCTA(A/G) motif recognized by LHP1 was present in a LHP1-target subset, which was enriched in the molecular function GO term “nucleic acid binding transcription factor activity”

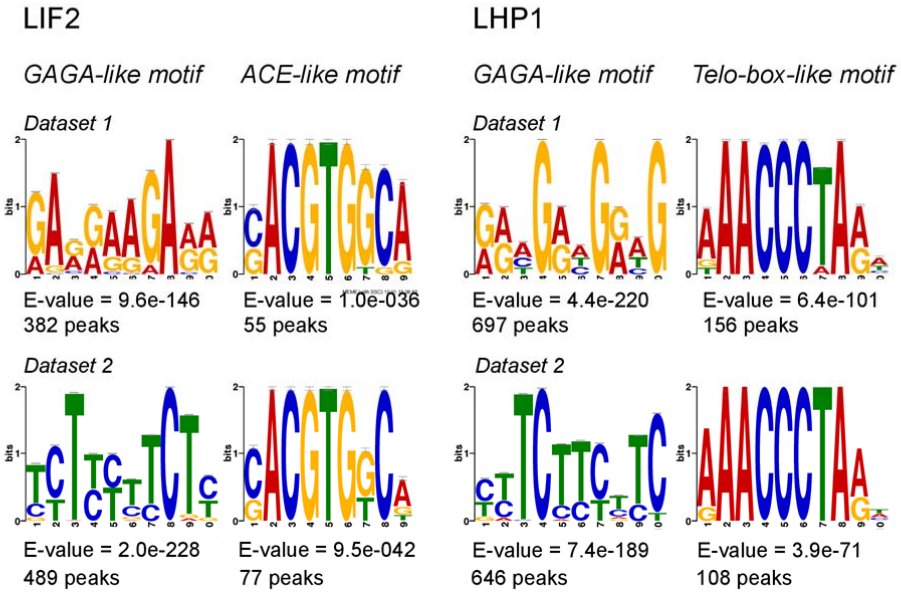

Figure 5: Identification of putative *cis*-regulatory DNA motifs in LIF2 ERs and LHP1 ERs.
The regions centered on LIF2 and LHP1 summits were used to screen for putative targeting motifs. The *E*-value of MEME program is an estimate of the expected number of motifs with the given log likelihood ratio (or higher), and with the same width and number of occurrences, that one would find in a similarly sized set of random sequences.

(GO:0001071, fold-enrichment 3.62, p-value 2.67 10^{-03}) and in the biological process GO term “carpel development” (GO:0048440, fold-enrichment >5, p-value 4.04 10^{-02})(Panther classification system), suggesting the existence of a small and specialized subset of LHP1 targets containing the (A/G/T)AACCCTA(A/G) *telo*-box-like

motif. Interestingly, *TELOMERE REPEAT BINDING PROTEIN1* (*TRB1*) also binds to the AAACCCTA motif and it was proposed that TRB1 may act as a transcriptional repressor in the absence of LHP1 (Zhou et al., 2015).

LIF2 has a major transcriptional activation activity on its targets

To better understand the mode of action of LIF2, we compared the binding profiles of LIF2 with our previous transcriptome data obtained from the seedlings and rosette leaves of *lif2* and *lhp1* mutants (Latrasse et al., 2011) (Figure 6). We observed a bias towards down-regulated genes among LIF2 targets (23.8%), suggesting that LIF2 had a global transcriptional activator role on its own targets. The *lif2* mutation had no significant impact on the transcription of LHP1 target genes, whereas LHP1 had a general repressor activity on LIF2 targets (25.5% of the LIF2 targets were deregulated in the *lhp1* mutant). A proportion of genes located in the LIF2-LHP1 IRs were activated by LIF2 and repressed by LHP1, suggesting that LIF2 and LHP1 have general antagonistic transcriptional roles in activation and repression, respectively. Nevertheless, small sets of LIF2-LHP1 IR genes were down-regulated in the mutants and enriched in stress response-associated GO terms (Figure 6 G), suggesting that LIF2 and LHP1 can also act synergistically to activate specific genes.

A complex interplay between LIF2 and LHP1 recruitments

To investigate the impact of LIF2 and LHP1 on each other's binding, we crossed the complemented mutant lines expressing tagged LIF2 or LHP1 with the *lif2-1 lhp1-4* double mutant and selected transgenic lines in single mutant backgrounds (named *lif2* LHP1 and *lhp1* LIF2). We performed ChIP-seq experiments and identified regions that exhibited differences in the binding of the tagged proteins compared with the binding in the original complemented mutant lines (*lif2* LIF2 and *lhp1* LHP1). The analysis revealed a strong bias towards a depletion of any protein binding in the double mutant background (Figure 7 A). In the absence of LHP1, LIF2 binding decreased strongly in regulatory regions (UTRs and promoters) and increased strongly in gene bodies (exons). Similar findings were observed for LHP1 (Figure 7 B). The gene set depleted in LIF2 binding in the *lhp1* background was enriched in stress-related genes, and in the GO term "transcription repressor activity" (GO:0016564, NF 17.1, p-value 8.9 10^{-07}; Supplemental Table 6). Since modifications of the binding of one protein at a precise locus in the mutant background could result from a direct loss of binding of the other or from indirect

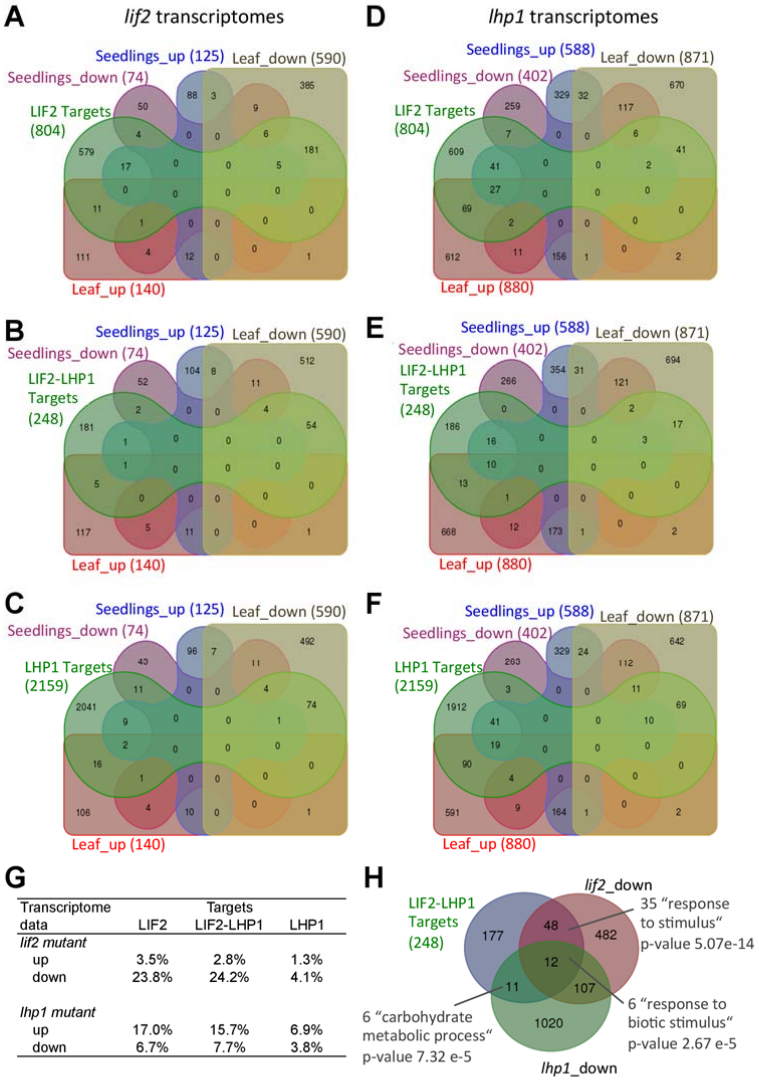

Transcriptome data	Targets LIF2	LIF2-LHP1	LHP1
lif2 mutant			
up	3.5%	2.8%	1.3%
down	23.8%	24.2%	4.1%
lhp1 mutant			
up	17.0%	15.7%	6.9%
down	6.7%	7.7%	3.8%

Figure 6: LIF2 functions mainly as a transcriptional activator on its targets.
(**A-F**) Venn diagrams between genes of LIF2 ERs (A, D), LIF2-LHP1 IRs (B, E, G) and LHP1 ERs (C, F) and deregulated genes in vegetative tissues of the *lif2* (A, B, C) and *lhp1* (D, E, F) mutants. The analysis involved genes for which the binding was located in CDSs or in UTRs.
(**G**) Comparisons between target genes and deregulated genes in *lif2* and *lhp1* mutants.
(**H**) Venn diagram and GO annotations of LHP1-LIF2 IR genes and genes activated by LHP1 and LIF2, respectively, revealed a small set of genes that requires a synergistic and activation function of both LIF2 and LHP1.

effects of its loss of function, we focused our analysis on the LIF2-LHP1 IR genes identified in the first part of this study (Figure 1). Among these LIF2-LHP1 IR genes, we identified three subsets that presented an alteration in LHP1 and LIF2 binding in the *lif2* LHP1 and *lhp1* LIF2 backgrounds (Figure 7 C). The three sets were enriched

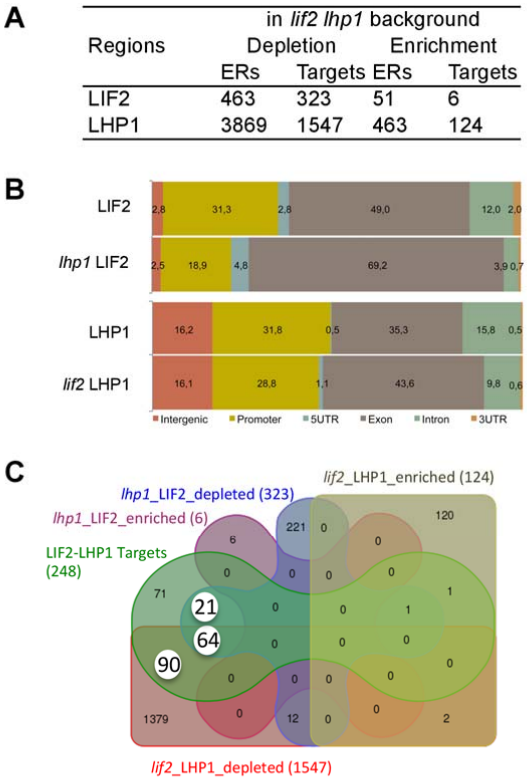

Figure 7: Complex interplay between LIF2 and LHP1 for their recruitment.
(**A**) LIF2 and LHP1 binding in the mutant backgrounds.
(**B**) Distribution of the annotations of the targeted regions.
(**C**) Venn diagram highlighting Set-21, Set-64 and Set-90 (white circles), which contain LIF2-LHP1 IR genes, depleted in one or the other protein, in the mutant backgrounds.

355 in stress response-associated GO terms (Supplemental Figure 8). In Set-64 (64
356 genes), the presence of both proteins was mutually required for their binding,
357 suggesting a synergistic mode of action, whereas for Set-90 and Set-21, LIF2 and
358 LHP1, respectively, were necessary for the presence of the other one. Therefore,

these data suggest a prominent role for LIF2 in LHP1 recruitment to chromatin and regulation in the LIF2-mediated stress response pathway. This role may be underestimated, as we only considered locations occupied by the two proteins under normal physiological conditions. Most of the genes of the three sets were not deregulated in our *lif2* and *lhp1* transcriptomes (Latrasse et al., 2011). This might be due to redundant mechanisms of gene regulation. Furthermore, transcriptome profiles, established in mutants under normal physiological conditions, may not highlight deregulation in responses to various cues. However, 45.3% of the Set-64 genes were down-regulated in *lif2,* in agreement with the major transcriptional activity of LIF2 (Supplemental Figure 8 D).

Rapid recruitment of LIF2 in response to methyl jasmonate

Due to the enrichment in stress GO terms, such as “JA-mediated signaling pathway”, in both *lif2* transcriptomes (Le Roux et al., 2014) and LIF2 ERs (Supplemental Figure 7), we investigated whether JA treatment affects LIF2 recruitment to chromatin by comparing ChIP-seq data obtained from plants subjected or not to JA treatment. For the JA treatment, we used a short-term (1 h) oxylipin-derived methyl jasmonate (MeJA) treatment to avoid complex downstream regulatory events, as a 1-h treatment was sufficient to transcriptionally activate JA-inducible marker genes in wild-type plants (Supplemental Figure 9). For each protein, we identified a reduced number of regions with binding modifications in response to MeJA (JA-ERs), and observed a bias toward enrichments in LIF2 and LHP1 in response to MeJA (Figure 8 A). Short-term MeJA treatment promoted LIF2 binding in promoter and intergenic regions and LHP1 binding at 5’ UTRs (Figure 8 B). Interestingly, after MeJA treatment, the ERs that exhibited the greatest enrichment in LIF2 or LHP1 were enriched in “transcription factor activity” GO term, and also in the “energy pathway” GO term for LIF2 ERs (Figure 8 C). When the JA ERs were compared to LIF2-LHP1 IRs under normal conditions, only a limited number of loci were identified, suggesting that we had access to very early regulatory events, in agreement with the observed enrichment in TFs, and/or that both proteins have independent functions in response to MeJA (Figure 8 D). Alternatively, the use of a gene set in which both proteins might already be present before the treatment introduced a bias in the analysis.

To further characterize LIF2 binding in response to MeJA, we examined the expression of JA-inducible genes, *MYC*2, *JASMONATE-ZIM DOMAIN* (*JAZ1, JAZ6*, *JAZ9*), *VEGETATIVE STORAGE PROTEIN2* (*VSP2*), and *LIPOXYGENASE3*

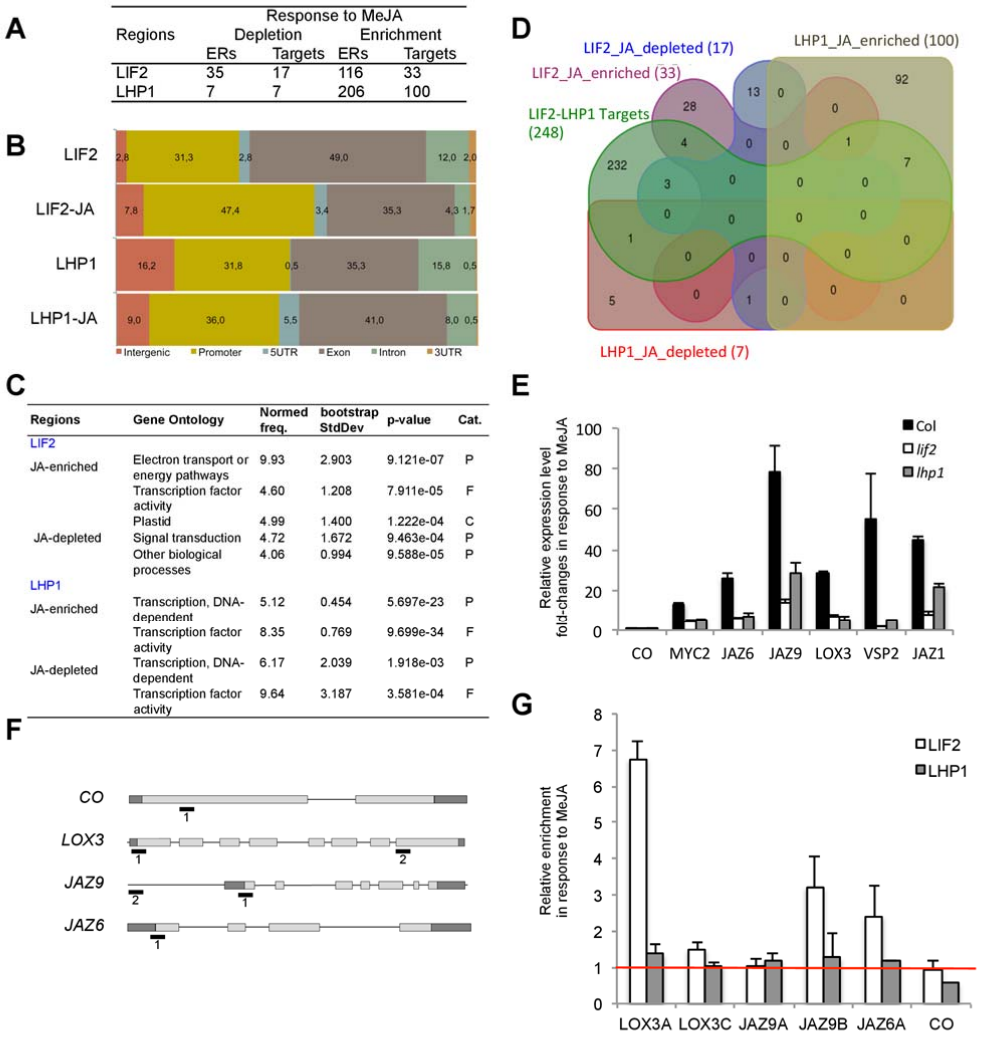

Figure 8: LIF2 and LHP1 binding in response to MeJA.
A 1-h MeJA treatment was performed on two-week-old seedlings.
(**A**) Dynamics of LIF2 and LHP1 binding in response to MeJA.
(**B**) Distribution of the annotations of the binding regions.
(**C**) GO terms with NF>4 (AgriGO toolkit). Cat.: category; P: process; F: function; C: cellular component.
(**D**) Venn diagram with the genes of the LIF2-LHP1 IRs.
(**E**) Fold changes of the relative expression in response to MeJA in the mutant backgrounds of stress-related genes. Mean±SEM. Three biological replicates were performed.
(**F-G**) Relative enrichments of LIF2 and LHP1 in response to MeJA. The targeted regions (i.e., 1, 2) are indicated in the schematic representation (F). ChIP-QPCR experiments (G). Three biological replicates were performed.

394 *(LOX3*). *LOX3* is among the bivalent genes identified by sequential ChIP (Luo et al.,
395 2012). These genes were up-regulated in wild-type, *lif2-1,* and *lhp1-4* plants in
396 response to MeJA treatment; however, the activation levels were higher in wild-type
397 plants than in any of the mutants (Figure 8 E). Under normal growth conditions, LIF2

and LHP1 were present on *LOX3*, a gene present in Set-64, whereas *JAZ6* and *JAZ9* were only targeted by LIF2 (our ChIP-seq data). These data suggested that the two proteins were cooperatively recruited to *LOX3* (our ChIP-seq data). Upon MeJA treatment, LIF2 binding increased in the TSS regions of the three loci, whereas LHP1 binding was not significantly affected (Figure 8 F). These data revealed that the early events of the transcriptional activation of the three JA-inducible genes require LIF2 recruitment. The presence of LHP1 on *LOX3* seemed to be required to reach a full level of activation, as suggested by *LOX3* expression in the *lhp1* mutant, but its distribution on the locus was not significantly affected. Therefore, LHP1 seems to be required for the early transcriptional events of JA-dependent activation of *LOX3* by LIF2. Whether long-term treatments would impact LHP1 binding requires further investigation.

Discussion

Dynamic switches that mediate the transition between active and inactive chromatin states are crucial for the development and adaptation of organisms. PRC and TRX complexes, with their antagonistic effects on transcriptional gene regulation, play a crucial role in these chromatin-associated transitions. Chromatin may be regarded as a bistable system composed of two main antagonistic chromatin states, and transitory intermediate chromatin states. The mechanism by which chromatin changes from one state to another remains poorly understood. To decipher this mechanism, we studied two interacting partners, LHP1, a plant PRC1 subunit, and the LIF2 hnRNP-Q protein. Our comparative analysis of their genome-wide binding profiles in wild-type and mutant backgrounds and under normal and stress conditions, and of their transcriptomes, revealed that these two proteins interact in a complex manner to control gene transcription.

Contrasting profiles were obtained for these interacting proteins: LHP1 was distributed over large genomic regions similar to histone marks, while LIF2 occurred in narrow binding regions, mainly located in promoters and in proximity to TSSs, which is reminiscent of TF binding at precise regulatory DNA elements. Furthermore, whereas LHP1 ERs were associated with the Polycomb H3K27me3 mark, as we previously reported using the DamID approach (Zhang et al., 2007), LIF2 was present in chromatin states characterized by the presence of H3K9ac and H3K4me3, which are usually associated with active/open chromatin.

The LIF2-LHP1 IRs were identified at the intersection of LIF2 and LHP1 protein distributions. However, to pursue and fully demonstrate that they are simultaneously binding to the exact same chromatin fiber, further analyses, such as sequential ChIP experiments, would be required. The LIF2-LHP1 IRs were associated with antagonistic marks, which may correspond to bivalent regions (Sequeira-Mendes et al., 2014) or to intermediate heterochromatin such as telomeric heterochromatin (Vrbsky et al., 2010; Vaquero-Sedas et al., 2012). Interestingly, 9.8% of the H3K9ac target genes in *A. thaliana* are also marked by H3K27me3 (Zhou et al., 2010; Karmodiya et al., 2012) and H3K9ac is present in bivalent chromatin regions of mouse promoters of developmentally regulated genes (Karmodiya et al., 2012). LHP1 interacts with MSI1 (Derkacheva et al., 2013), which associates with histone deacetylase 19 (HDAC19) in the same *in vivo* complex, to maintain a low H3K9ac level at genes involved in the ABA signalling pathway (Mehdi et al., 2015). Furthermore, the LIF2-LHP1 IRs had a good coverage with Chromatin State 2 and

were enriched in stress-responsive genes, demonstrating that the LIF2/LHP1 duo seems to have a specialized function in the stress response pathway and a putative role in maintaining or regulating a distinctive chromatin state at a specific gene set. Furthermore, the binding maps of each protein, established in the absence of its partner, revealed various scenarios that were highly dependent on the genomic contexts, with synergistic binding, as well as binding dependent on one or the other protein.

The identification of GAGA motifs in LHP1 ERs confirmed a recent discovery (Hecker et al., 2015). Indeed, the BASIC PENTACYSTEINE6 (BPC6) GAGA-binding factor interacts with LHP1 and recruits LHP1 at GAGA motif-containing DNA probes *in vitro* (Hecker et al., 2015). Interestingly, GAGA motifs were also present in FIE ERs [10], as was Motif 2, which is similar to a *telo*-like box. The presence of these two types of motifs in LHP1 and FIE ERs suggests the existence of common recruitment motifs between plant PRC1 and PRC2 subunits, but also between PRC1 and LIF2. Thus, these different DNA motifs may correspond to modules that participate to form putative plant PREs.

In addition to establishing the global rules governing LIF2 and LHP1 binding, we observed that the two proteins exhibited different recruitment dynamics in response to a short-term MeJA treatment. A rapid increase in LIF2 binding was observed, especially at the TSS of *LOX3*, *JAZ6,* and *JAZ9*, with an associated increase in gene expression. These data were in agreement with the global down-regulation of LIF2 targets in *lif2*. At *LOX3,* the presence of LHP1 was not modulated by the MeJA treatment, but LHP1 was required for LIF2-mediated activation. Removal of LHP1 was not a prerequisite for the early transcriptional activation, suggesting that the two proteins may have different kinetics of action. Thus, one hypothesis would be that the RNA-binding protein LIF2 functions in transcriptional activation, especially in JA-dependent activation, and may counteract gene repression via its interaction with LHP1. Further investigation is needed to understand this dynamic and complex interplay. For instance, it remains unclear how LIF2 specifically interacts with chromatin. Perhaps this interaction is mediated by RRMs. Indeed, RRMs are plastic protein domains and some RRMs also have DNA-binding properties (Enokizono et al., 2005; Grinstein et al., 2007; Wan et al., 2007). Alternatively, RNA molecules interacting with RRMs may participate in RNA/DNA recognition, and thus help target RBP via their interaction with RNA molecules. Since RNA molecules play diverse functions in modulating animal PRC activities, further investigation of putative

interactions between LIF2 and RNA molecules will be of key importance.

Finally, we showed that LHP1 ERs had a significant and robust tendency to form clusters (in the ~10 kb range), regardless of the chromosome arm identity. Due to the large number of LHP1 ERs in the genome, the distribution of LHP1 clusters may not be neutral and may influence the functional organization of the genome. Indeed, proteins in the HP1 family have dimerization properties and SWI6 even has an oligomerization property, which contributes to heterochromatin formation (Canzio et al., 2011). Thus a clustering of the LHP1 ERs may have 3D consequences on genome organization. In animals, PcG proteins contribute to the modular organization of the linear epigenome, but also to the 3D genome organization (Cavalli, 2014; Del Prete et al., 2015). In *A. thaliana,* recent HiC studies highlighted long-range genome interactions, but the absence of large chromatin modules as observed in animal genomes (Feng et al., 2014; Grob et al., 2014), possibly due to resolution limitations. Although restricted to one dimension, our approach in this study, in which spatial statistics are applied to genome-wide data, represents a complementary tool for deciphering eukaryotic genome organization. It allowed us to evaluate distribution patterns of chromatin-associated proteins at different scales and highlighted the existence of short-range clusters on the linear organization of the *A. thaliana* genome. It will be interesting to determine whether the linear proximity of LHP1 ERs contributes to the formation of LHP1 foci (Gaudin et al., 2001), promotes silent plant chromatin formation, or influences the 3D genome organization.

Methods

Materials and hormonal treatment

All *Arabidopsis thaliana* lines used in this study are in the Col-0 background. The *lif2-1* and *lhp1-4* mutants were previously described (Latrasse et al., 2011). For all experiments, plants were grown *in vitro* for 14 days under controlled long-day conditions as previously described (Gaudin et al., 2001). For methyl jasmonate (MeJA) treatments a filter paper was imbibed with 10 µl of 95% MeJA (Sigma-Aldrich, Ref. 392707) and placed in a Petri dish. Plates were hermetically sealed and placed for 1 h under identical growth conditions. MeJA treated and mock seedlings were either directly harvested for gene expression analyses or fixed for ChIP assays after the 1-h treatment. All primers are listed in Supplemental Table 7.

Plasmid constructs

For the 3xHA:LIF2 binary construct, the 3xHA tag was PCR amplified from the pGWB15 vector (Invitrogen) using the 3HA-1 and 3HA-2 primers bearing *Pst*I and *Xba*I restriction sites, respectively. After digestion and purification, the 3xHA fragment was inserted into the pCambia1300 vector giving the pCa-HA vector. The Nos terminator, amplified from plasmid pUC-SPYNE (Walter et al., 2004) using the Nost-1 and Nost-2 primers (bearing *Kpn*I and *EcoR*I sites, respectively) was digested, gel-purified, and inserted into the *Kpn*I/*EcoR*I digested pCa-HA vector. A 3-kbp promoter region of *LIF2* (including the first three codons) was amplified from the T18A10 BAC plasmid (ABRC DNA stock center) using primers AD379-28 and AD379-29 (bearing a *Pst*I restriction site). The *Pst*I-digested LIF2 promoter fragment was gel-purified and inserted into the pCa-HA-tNos vector at the *Pst*I and blunt-made *Hind*III sites. Finally, the *LIF2* genomic region was amplified from T18A10 using the primers AD379-30 and AD379-32, digested with *Xho*I and inserted into the *Sal*I/*Sma*I-digested pCa-ProLIF2:HA-tNos vector giving the pCa-ProLIF2:HA:LIF2-tNos vector (N-terminal HA-tagged gLIF2).

For the ProLHP1:LHP1:HA binary construct, a 3xHA fragment was PCR amplified from the pGWB15 vector (Invitrogen) using the 3HA-2 and 3HA-2 primers and digested with *EcoR*V and *Xho*I. The 3xHA fragment was inserted into the *EcoR*V restriction site of the vector bearing a 5569-bp genomic LHP1 fragment (Latrasse et al., 2011). Subsequently, the *Nco*I/*Bst*EII fragment containing the LHP1:3xHA-tagged region was substituted to the wild-type genomic fragment of the pCaSSP vector

giving the gLHP1:HA binary plasmid (C-terminal HA tagged gLHP1). All subcloning steps were confirmed by sequencing. Col-0 plants were transformed by floral dip. For each construct, homozygous transgenic lines with wild-type phenotypes were selected, in which the functional HA-tagged protein was detected.

RNA extraction

Total RNA was isolated from 14-day-old *in vitro*-grown seedlings, subjected or not to MeJA treatment, using the RNeasy Plant Mini Kit (QIAGEN) according to supplier's instructions. Total RNA (1-2 µg) was treated with RNase-free DNaseI (Invitrogen) and reverse transcribed with Superscript II reverse transcriptase (Invitrogen).

Quantitative real-time PCR

Relative levels of cDNA (RT-qPCR) and immunoprecipitated DNA fragments (ChIP-qPCR) were analyzed by quantitative real-time PCR on an Eppendorf Mastercycler®ep Realplex using SsoAdvancedTM SYBR® (Biorad). Immunoprecipitated DNA levels were normalized to input and to the internal reference gene *EF1* (AT5G60390). The cDNA levels were normalized to *EF1*.

ChIP library construction and sequencing

ChIP assays were performed on five grams of 14-day-old *in vitro* seedlings from transgenic lines expressing LHP1-HA or LIF2-HA in the single or double mutant genetic backgrounds, using a previously published protocol (Latrasse et al., 2011), with the following minor modifications. Chromatin was immunoprecipitated overnight using high affinity anti-HA antibody (Roche, Ref. 11867423001). Immunoprecipitated DNA enrichment was controlled by quantitative real-time PCR (qPCR). DNA quantity and quality were checked using a Qubit fluorometer (ThermoFisher Scientific, Waltham, MA) and Agilent 2100 Bioanalyzer (Agilent Technologies, Santa Clara, CA). Several independent experiences were pooled for library construction. Then, 10-15 ng of immunoprecipitated DNA was fragmented to a 100-500 bp range using the E210 Covaris instrument (Covaris, Woburn, MA). Libraries were prepared according to the Illumina standard procedure using the NEBNext DNA Sample Preparation Reagent Set 1 (New England Biolabs, Ipswich, MA) and homemade ligation adaptors. The ligated product was amplified by 12 cycles of PCR using Platinum Pfx DNA Polymerase (ThermoFisher Scientific). Amplified material was

purified using Agencourt Ampure XP beads (Beckmann Coulter Genomics, Danvers, MA). Libraries were then quantified by qPCR and library profiles were evaluated using an Agilent 2100 Bioanalyzer. Two independent libraries for each protein were sequenced using 100 base-length read chemistry in a paired-end flow cell on the HiSeq2000 (Illumina, San Diego, CA).

ChIP-seq data analyses

After Illumina sequencing, Illumina read processing and quality filtering were performed. An in-house quality control process was applied to reads that passed the Illumina quality filters. Low quality nucleotides (Q < 20) were discarded from both ends of the reads. Next, Illumina adapter and primer sequences were removed from the reads. Then, reads shorter than 30 nucleotides after trimming were discarded. These trimming and removing steps were achieved using internal software based on the FastX package (FASTX-Toolkit, http://hannonlab.cshl.edu/fastx_toolkit/index.html). This processing yields high quality data and improves subsequent analyses. The sequencing reads were uniquely mapped to the Arabidopsis genome (TAIR10; http://www.arabidopsis.org) using Bowtie 4.1.2 mapper (Langmead et al., 2009) with default mismatch parameters, and retaining only reads mapping uniquely to the genome for further analysis. The main heterochromatic regions of the genome were thus excluded from our analysis.

To identify biologically relevant binding regions, peak prediction and normalization were performed using MACS1.4.1 (Zhang et al., 2008) and peak analysis was performed using S-MART (Langmead et al., 2009) or the “annotatePeaks.pl” software from Homer (http://homer.salk.edu/homer; Heinz et al., 2010). High-confidence target regions (i.e., enriched regions, ERs) were defined as strict overlap of the MACS peaks from the corresponding biological replicates.

By default, a TSS region was defined from -1 kb to +100 bp from TSS and the TTS region was defined from -100 bp to +1 kb from the TTS. The process of annotating peaks/regions was divided into two primary parts. The first determined the distance to the nearest TSS and assigned the peak to that gene. The second determined the genomic annotation of the region occupied by the center of the peak/region.

Bioinformatics analyses

Motifs were predicted using the integrated online pipeline “peak-motifs” (http://plants.rsat.eu/; Thomas-Chollier et al., 2011; Thomas-Chollier et al., 2012). Briefly, 50 and 300 bp surrounding protein-binding summits were scanned for a global overrepresentation of words (oligo-analyses) or spaced words (dyad-analyses). Then, 5000 random, artificial 300-bp long sequences were generated by the "RSAT-random sequence tool" (http://plants.rsat.eu/) and were used as background control for motif discovery. In parallel, sequences were analyzed by the motif prediction program "MEME" (Bailey and Elkan, 1995). The word occurrence was determined using the word frequency program in AtcisDB from AGRIS (http://arabidopsis.med.ohio-state.edu/AtcisDB/).

The functional annotation and classification of gene populations was carried out using the online "AgriGO" gene Ontology tool (http://bioinfo.cau.edu.cn/agriGO/) using pre-set parameters. Venn diagrams were generated using the online tool provided by T. Hulsen (http://bioinformatics.psb.ugent.be/webtools/Venn/).

To analyze the histone mark enrichments over the ERs, ChIP-seq data presented in (Luo et al., 2012) were used and available at SRA under IDs GSM701923-701931. Raw data were mapped onto the TAIR10 genome with the Bowtie mapper (Langmead et al., 2009) (unique hits, 1 mismatch at most). Mapped reads were processed using SAMtools (Li et al., 2009) and BEDtools (Quinlan and Hall, 2010). The number of reads per bp of the selected loci was counted and compared with that of randomized loci (using the shuffle BEDtool). Fold enrichment/depletion was calculated as the ratio between the mean read number in regions of interest versus randomized regions. Statistical significance was assessed by t-tests. Boxplots represent distribution of histone mark ChIP-seq reads within LIF2, LHP1, LIF2-LHP1, and the corresponding randomized regions.

Spatial distributions of the targeted regions

The spatial distributions of LHP1 and LIF2 targeted regions were quantified and analyzed for each individual biological replicate, using the cumulative distribution functions of (1) the distance to the nearest neighbor of each targeted region and (2) the inter-distance between every pair of targeted regions. Departure from randomness was assessed by adapting a Monte Carlo procedure developed for 3D data (Andrey et al., 2010). Observed distributions were compared to distributions obtained under complete randomization of targeted regions without overlap (999

randomizations for computing averages of distance functions under randomness, 999 further randomizations for computing envelopes around averages). The relative position of the empirical distance function within the range of variations under randomness was used to estimate p-values (Andrey et al., 2010).

Accession Numbers

Sequencing data were deposited at NCBI, under the Sequence Read Archive (SRA) number SRP068984.

Supplemental data

Supplemental Figure 1: ChIP-seq experiments.

Supplemental Figure 2: Exon distributions of LIF2 ERs.

Supplemental Figure 3: Distributions of the number of summits in 1-Mb windows.

Supplemental Figure 4: Cumulative distribution of the distance to the nearest LHP1 summit.

Supplemental Figure 5: Cumulative distribution of LHP1 summit inter-distances.

Supplemental Figure 6: Post-translational histone modifications and their distributions in LIF2 ERs, LHP1 ERs and LIF2-LHP1 IRs.

Supplemental Figure 7: GO term analysis of the target loci of LIF2 and LHP1.

Supplemental Figure 8: Analyses of the LIF2-LHP1 IRs with binding alterations in the mutant backgrounds.

Supplemental Figure 9: Expression kinetics of JA-induced marker genes in response to MeJA treatment in wild-type plants.

Supplemental Table 1: Tandem duplications and LHP1 target genes.

Supplemental Table 2: GO term analysis of the genes present in LIF2 ERs and LIF2-LHP1 IRs using the Plant Functional Genomics (BAR) classification Superviewer program.

Supplemental Table 3: Enrichments of LIF2 and LHP1 targets in specific transcription factor families using the PlantGSEA resource.

Supplemental Table 4: LIF2 and LHP1 targets are also bound by specific transcription factors.

Supplemental Table 5: Occurrences of the two identified DNA words.

Supplemental Table 6: GO term analysis of LIF2 or LHP1 depleted regions in the mutant backgrounds (AgriGO).

Supplemental Table 7: List of primers.

Acknowledgments

We thank Bruno Letarnec and Hervé Ferry for plant care in the greenhouses, Dr. Georg Haberer for providing the S-cluster listing and Dr. Crisanto Gutierrez for helpful exchange. We are grateful to our colleagues, Dr. Franziska Turck and Dr. Dierk Wanke, for critical reading of the manuscript and suggestions. D.L., A.M. and M.H. were supported by fellowships from the ANR (ANR-08-BLAN-0200, Polycombara) from the French Research Ministry. S.D.L. was supported by a PhD fellowship provided by the European Commission Seventh Framework-People-2012-ITN project EpiTRAITS (Epigenetic regulation of economically important plant traits, no-316965). The Génoscope supported the sequencing in the frame of a large-scale DNA sequencing project (N°11). The IJPB benefits from the support of the LabEx Saclay Plant Sciences-SPS (ANR-10-LABX-0040-SPS).

Author contributions

A.M., D.L., M.Z., P.A., N.H.H., M.H., C.B., S.D.P., A.A., V.G. performed the experiments. A.M., M.Z., M.Z., P.A., M.H., H.Q., V.G. analyzed the data. A.M., M.Z.,

P.A., V.G. prepared the figures. A.M., V.G. wrote the manuscript.

Competing financial interests

The authors declare no competing financial interests.

Figure legends

Figure 1: Genome-wide distributions of LIF2 and LHP1.
(**A**) Chromosomal view of the peaks using model-based analysis.
(**B**) Screenshot of a 100-kb window with the distributions.
(**C**) Size distributions of the ERs defined as intersects of MACS peaks for the biological replicates.
(**D**) Distributions of ER-associated annotations (percentage). Regions with identical sizes were randomly shuffled in the genome and compared with the observed ERs, using a Fisher's exact test.
(**E**) Distributions of IP enrichment (log2(# reads IP/ # read input)) over the transcript structures.
(**F**) Distance to closest transcriptional start sites (TSS) of LIF2 and LHP1 ERs, and the corresponding randomized regions.

Figure 2: Non-random distributions of the LHP1 ERs and LIF2 ERs in the *A. thaliana* genome.
(**A**) Number of summits in 1-Mb windows along Chromosome 1.
(**B-D**) Observed (pink) and random model (black: average; grey: 95% envelope) distributions of distance to nearest ER (B-C) and of all ER inter-distances (D) on the first arm of Chromosome 1. Similar results were obtained for all chromosome arms (Supplemental Figures 3, 4 and 5).

Figure 3. Post-translational histone modifications (PTMs) and the H2A.Z histone variant in the LIF2-ERs, LHP1 ERs, and LIF2-LHP1 IRs.
(**A**) Heat map presenting the fold changes (p-value paired t-test) between targeted and randomized regions.

(**B**) Percentage of chromatin states 2 and 4 (CS2 and CS4; defined by Sequeira-Mendes et al., 2014) covering LHP1 ERs, LIF2 ERs, LIF2-LHP1 IRs, and randomized control regions.

Figure 4: LIF2 binds preferentially stress-response genes.
(**A**) Average gene responsiveness scores were calculated based on a published data set (Aceituno et al., 2008) and normalized to the genome-wide average.
(**B**) GO analysis of LIF2 ERs and LIF2-LHP1 IRs using the AgriGO toolkit. The biological process GO terms, with the 25 best normed frequencies (NF) and with NF≥1.5 are presented for LIF2 ERs and LIF2-LHP1 IRs, respectively.

Figure 5: Identification of putative *cis*-regulatory DNA motifs in LIF2 ERs and LHP1 ERs.
The regions centered on LIF2 and LHP1 summits were used to screen for putative targeting motifs. The *E*-value of MEME program is an estimate of the expected number of motifs with the given log likelihood ratio (or higher), and with the same width and number of occurrences, that one would find in a similarly sized set of random sequences.

Figure 6: LIF2 functions mainly as a transcriptional activator on its targets.
(**A-F**) Venn diagrams between genes of LIF2 ERs (A, D), LIF2-LHP1 IRs (B, E, G), and LHP1 ERs (C, F) and deregulated genes in vegetative tissues of the *lif2* (A, B, C) and *lhp1* (D, E, F) mutants. The analysis involved genes for which the binding was located in CDSs or in UTRs.
(**G**) Comparisons between target genes and deregulated genes in *lif2* and *lhp1* mutants.
(**H**) Venn diagram and GO annotations of LHP1-LIF2 IR genes and genes activated by LHP1 and LIF2, respectively, revealed a small set of genes that requires a synergistic and activation function of both LIF2 and LHP1.

Figure 7: Complex interplay between LIF2 and LHP1 for their recruitment.
(**A**) LIF2 and LHP1 binding in the mutant backgrounds.
(**B**) Distribution of the annotations of the targeted regions.

(**C**) Venn diagram highlighting Set-21, Set-64, and Set-90 (white circles), which contain LIF2-LHP1 IR genes, depleted in one or the other protein, in the mutant backgrounds.

Figure 8: LIF2 and LHP1 binding in response to MeJA.

A 1-h MeJA treatment was performed on two-week-old seedlings.

(**A**) Dynamics of LIF2 and LHP1 binding in response to MeJA.

(**B**) Distribution of the annotations of the binding regions.

(**C**) GO terms with NF>4 (AgriGO toolkit). Cat.: category; P: process; F: function; C: cellular component.

(**D**) Venn diagram with the genes of the LIF2-LHP1 IRs.

(**E**) Fold changes of the relative expression in response to MeJA in the mutant backgrounds of stress-related genes. Mean±SEM. Three biological replicates were performed.

(**F-G**) Relative enrichments of LIF2 and LHP1 in response to MeJA. The targeted regions (i.e., 1, 2) are indicated in the schematic representations (F). ChIP-QPCR experiments (G). Three biological replicates were performed.

Parsed Citations

Aceituno, F.F., Moseyko, N., Rhee, S.Y., and Gutierrez, R.A. (2008). The rules of gene expression in plants: organ identity and gene body methylation are key factors for regulation of gene expression in Arabidopsis thaliana. BMC Genomics 9, 438.

Pubmed: Author and Title
CrossRef: Author and Title
Google Scholar: Author Only Title Only Author and Title

Andrey, P., Kieu, K., Kress, C., Lehmann, G., Tirichine, L., Liu, Z., Biot, E., Adenot, P.G., Hue-Beauvais, C., Houba-Herin, N., Duranthon, V., Devinoy, E., Beaujean, N., Gaudin, V., Maurin, Y., and Debey, P. (2010). Statistical analysis of 3D images detects regular spatial distributions of centromeres and chromocenters in animal and plant nuclei. PLoS Computational Biology 6, e1000853.

Pubmed: Author and Title
CrossRef: Author and Title
Google Scholar: Author Only Title Only Author and Title

Bailey, T.L., and Elkan, C. (1995). The value of prior knowledge in discovering motifs with MEME. Proc Int Conf Intell Syst Mol Biol 3, 21-29.

Pubmed: Author and Title
CrossRef: Author and Title
Google Scholar: Author Only Title Only Author and Title

Bauer, M., Trupke, J., and Ringrose, L. (2015). The quest for mammalian Polycomb response elements: are we there yet? Chromosoma.

Brockdorff, N. (2013). Noncoding RNA and Polycomb recruitment. RNA 191, 429-442.

Pubmed: Author and Title
CrossRef: Author and Title
Google Scholar: Author Only Title Only Author and Title

Calonje, M. (2014). PRC1 marks the difference in plant PcG repression. Molecular Plant 7, 459-471.

Pubmed: Author and Title
CrossRef: Author and Title
Google Scholar: Author Only Title Only Author and Title

Canzio, D., Chang, E.Y., Shankar, S., Kuchenbecker, K.M., Simon, M.D., Madhani, H.D., Narlikar, G.J., and Al-Sady, B. (2011). Chromodomain-mediated oligomerization of HP1 suggests a nucleosome-bridging mechanism for heterochromatin assembly. Molecular Cell 41, 67-81.

Pubmed: Author and Title
CrossRef: Author and Title
Google Scholar: Author Only Title Only Author and Title

Cavalli, G. (2014). Chromosomes: now in 3D! Nature Reviews Molecular Cell Biology 15, 6.

Pubmed: Author and Title
CrossRef: Author and Title
Google Scholar: Author Only Title Only Author and Title

Chen, D., Xu, G., Tang, W., Jing, Y., Ji, Q., Fei, Z., and Lin, R. (2013). Antagonistic basic helix-loop-helix/bZIP transcription factors form transcriptional modules that integrate light and reactive oxygen species signaling in Arabidopsis. The Plant Cell 25, 1657-1673.

Pubmed: Author and Title
CrossRef: Author and Title
Google Scholar: Author Only Title Only Author and Title

Coleman-Derr, D., and Zilberman, D. (2012). Deposition of histone variant H2A.Z within gene bodies regulates responsive genes. PLoS Genetics 8, e1002988.

Pubmed: Author and Title
CrossRef: Author and Title
Google Scholar: Author Only Title Only Author and Title

Csorba, T., Questa, J.I., Sun, Q., and Dean, C. (2014). Antisense COOLAIR mediates the coordinated switching of chromatin states at FLC during vernalization. Proceedings of the National Academy of Sciences of the United States of America 111, 16160-16165.

Pubmed: Author and Title
CrossRef: Author and Title
Google Scholar: Author Only Title Only Author and Title

Del Prete, S., Mikulski, P., Schubert, D., and Gaudin, V. (2015). One, Two, Three: Polycomb Proteins Hit All Dimensions of Gene Regulation. Genes 6, 520-542.

Pubmed: Author and Title
CrossRef: Author and Title
Google Scholar: Author Only Title Only Author and Title

Deng, W., Buzas, D.M., Ying, H., Robertson, M., Taylor, J., Peacock, W.J., Dennis, E.S., and Helliwell, C. (2013). Arabidopsis Polycomb Repressive Complex 2 binding sites contain putative GAGA factor binding motifs within coding regions of genes. BMC Genomics 14, 593.

Pubmed: Author and Title
CrossRef: Author and Title
Google Scholar: Author Only Title Only Author and Title

Derkacheva, M., Steinbach, Y., Wildhaber, T., Mozgova, I., Mahrez, W., Nanni, P., Bischof, S., Gruissem, W., and Hennig, L. (2013). Arabidopsis MSI1 connects LHP1 to PRC2 complexes. The EMBO journal 32, 2073-2085.
Pubmed: Author and Title
CrossRef: Author and Title
Google Scholar: Author Only Title Only Author and Title

Enokizono, Y., Konishi, Y., Nagata, K., Ouhashi, K., Uesugi, S., Ishikawa, F., and Katahira, M. (2005). Structure of hnRNP D complexed with single-stranded telomere DNA and unfolding of the quadruplex by heterogeneous nuclear ribonucleoprotein D. The Journal of biological chemistry 280, 18862-18870.
Pubmed: Author and Title
CrossRef: Author and Title
Google Scholar: Author Only Title Only Author and Title

Feng, S., Cokus, S.J., Schubert, V., Zhai, J., Pellegrini, M., and Jacobsen, S.E. (2014). Genome-wide Hi-C analyses in wild-type and mutants reveal high-resolution chromatin interactions in Arabidopsis. Molecular Cell 55, 694-707.
Pubmed: Author and Title
CrossRef: Author and Title
Google Scholar: Author Only Title Only Author and Title

Forderer, A., Zhou, Y., and Turck, F. (2016). The age of multiplexity: recruitment and interactions of Polycomb complexes in plants. Current Opinion in Plant Biology 29, 169-178.
Pubmed: Author and Title
CrossRef: Author and Title
Google Scholar: Author Only Title Only Author and Title

Gaspin, C., Rami, J.F., and Lescure, B. (2010). Distribution of short interstitial telomere motifs in two plant genomes: putative origin and function. BMC plant biology 10, 283.
Pubmed: Author and Title
CrossRef: Author and Title
Google Scholar: Author Only Title Only Author and Title

Gaudin, V., Libault, M., Pouteau, S., Juul, T., Zhao, G., Lefebvre, D., and Grandjean, O. (2001). Mutations in LIKE HETEROCHROMATIN PROTEIN 1 affect flowering time and plant architecture in Arabidopsis. Development 128, 4847-4858.
Pubmed: Author and Title
CrossRef: Author and Title
Google Scholar: Author Only Title Only Author and Title

Gil, J., and O'Loghlen, A. (2014). PRC1 complex diversity: where is it taking us? Trends in Cell Biology 24, 632-641.
Pubmed: Author and Title
CrossRef: Author and Title
Google Scholar: Author Only Title Only Author and Title

Grinstein, E., Du, Y., Santourlidis, S., Christ, J., Uhrberg, M., and Wernet, P. (2007). Nucleolin regulates gene expression in CD34-positive hematopoietic cells. The Journal of biological chemistry 282, 12439-12449.
Pubmed: Author and Title
CrossRef: Author and Title
Google Scholar: Author Only Title Only Author and Title

Grob, S., Schmid, M.W., and Grossniklaus, U. (2014). Hi-C analysis in Arabidopsis identifies the KNOT, a structure with similarities to the flamenco locus of Drosophila. Molecular Cell 55, 678-693.
Pubmed: Author and Title
CrossRef: Author and Title
Google Scholar: Author Only Title Only Author and Title

Haberer, G., Hindemitt, T., Meyers, B.C., and Mayer, K.F. (2004). Transcriptional similarities, dissimilarities, and conservation of cis-elements in duplicated genes of Arabidopsis. Plant physiology 136, 3009-3022.
Pubmed: Author and Title
CrossRef: Author and Title
Google Scholar: Author Only Title Only Author and Title

Hecker, A., Brand, L.H., Peter, S., Simoncello, N., Kilian, J., Harter, K., Gaudin, V., and Wanke, D. (2015). The Arabidopsis GAGA-Binding Factor BASIC PENTACYSTEINE6 Recruits the POLYCOMB-REPRESSIVE COMPLEX1 Component LIKE HETEROCHROMATIN PROTEIN1 to GAGA DNA Motifs. Plant physiology 168, 1013-1024.
Pubmed: Author and Title
CrossRef: Author and Title
Google Scholar: Author Only Title Only Author and Title

Heinz, S., Benner, C., Spann, N., Bertolino, E., Lin, Y.C., Laslo, P., Cheng, J.X., Murre, C., Singh, H., and Glass, C.K. (2010). Simple combinations of lineage-determining transcription factors prime cis-regulatory elements required for macrophage and B cell identities. Molecular Cell 38, 576-589.
Pubmed: Author and Title
CrossRef: Author and Title
Google Scholar: Author Only Title Only Author and Title

Heo, J.B., and Sung, S. (2011). Vernalization-mediated epigenetic silencing by a long intronic noncoding RNA. Science 331, 76-79.
Pubmed: Author and Title
CrossRef: Author and Title
Google Scholar: Author Only Title Only Author and Title

Karmodiya, K., Krebs, A.R., Oulad-Abdelghani, M., Kimura, H., and Tora, L. (2012). H3K9 and H3K14 acetylation co-occur at many

gene regulatory elements, while H3K14ac marks a subset of inactive inducible promoters in mouse embryonic stem cells. BMC Genomics 13, 424.
Pubmed: Author and Title
CrossRef: Author and Title
Google Scholar: Author Only Title Only Author and Title

Langmead, B., Trapnell, C., Pop, M., and Salzberg, S.L. (2009). Ultrafast and memory-efficient alignment of short DNA sequences to the human genome. Genome Biology 10, R25.
Pubmed: Author and Title
CrossRef: Author and Title
Google Scholar: Author Only Title Only Author and Title

Latrasse, D., Germann, S., Houba-Herin, N., Dubois, E., Bui-Prodhomme, D., Hourcade, D., Juul-Jensen, T., Le Roux, C., Majira, A., Simoncello, N., Granier, F., Taconnat, L., Renou, J.P., and Gaudin, V. (2011). Control of flowering and cell fate by LIF2, an RNA binding partner of the polycomb complex component LHP1. PLoS One 6, e16592.
Pubmed: Author and Title
CrossRef: Author and Title
Google Scholar: Author Only Title Only Author and Title

Le Roux, C., Del Prete, S., Boutet-Mercey, S., Perreau, F., Balague, C., Roby, D., Fagard, M., and Gaudin, V. (2014). The hnRNP-Q protein LIF2 participates in the plant immune response. PLoS One 9, e99343.
Pubmed: Author and Title
CrossRef: Author and Title
Google Scholar: Author Only Title Only Author and Title

Lee, J., He, K., Stolc, V., Lee, H., Figueroa, P., Gao, Y., Tongprasit, W., Zhao, H., Lee, I., and Deng, X.W. (2007). Analysis of transcription factor HY5 genomic binding sites revealed its hierarchical role in light regulation of development. The Plant Cell 19, 731-749.
Pubmed: Author and Title
CrossRef: Author and Title
Google Scholar: Author Only Title Only Author and Title

Li, H., Handsaker, B., Wysoker, A., Fennell, T., Ruan, J., Homer, N., Marth, G., Abecasis, G., and Durbin, R. (2009). The Sequence Alignment/Map format and SAMtools. Bioinformatics 25, 2078-2079.
Pubmed: Author and Title
CrossRef: Author and Title
Google Scholar: Author Only Title Only Author and Title

Luo, C., Sidote, D.J., Zhang, Y., Kerstetter, R.A., Michael, T.P., and Lam, E. (2012). Integrative analysis of chromatin states in Arabidopsis identified potential regulatory mechanisms for natural antisense transcript production. The Plant journal : for cell and molecular biology.
Pubmed: Author and Title
CrossRef: Author and Title
Google Scholar: Author Only Title Only Author and Title

Mehdi, S., Derkacheva, M., Ramstrom, M., Kralemann, L., Bergquist, J., and Hennig, L. (2015). MSI1 functions in a HDAC complex to fine-tune ABA signaling. The Plant Cell.
Pubmed: Author and Title
CrossRef: Author and Title
Google Scholar: Author Only Title Only Author and Title

Provart, N.J., Gil, P., Chen, W., Han, B., Chang, H.S., Wang, X., and Zhu, T. (2003). Gene expression phenotypes of Arabidopsis associated with sensitivity to low temperatures. Plant physiology 132, 893-906.
Pubmed: Author and Title
CrossRef: Author and Title
Google Scholar: Author Only Title Only Author and Title

Pu, L., and Sung, Z.R. (2015). PcG and trxG in plants - friends or foes. Trends Genetics 31, 252-262.
Pubmed: Author and Title
CrossRef: Author and Title
Google Scholar: Author Only Title Only Author and Title

Quinlan, A.R., and Hall, I.M. (2010). BEDTools: a flexible suite of utilities for comparing genomic features. Bioinformatics 26, 841-842.
Pubmed: Author and Title
CrossRef: Author and Title
Google Scholar: Author Only Title Only Author and Title

Regad, F., Lebas, M., and Lescure, B. (1994). Interstitial telomeric repeats within the Arabidopsis thaliana genome. Journal of Molecular Biology 239, 163-169.
Pubmed: Author and Title
CrossRef: Author and Title
Google Scholar: Author Only Title Only Author and Title

Sequeira-Mendes, J., Araguez, I., Peiro, R., Mendez-Giraldez, R., Zhang, X., Jacobsen, S.E., Bastolla, U., and Gutierrez, C. (2014). The Functional Topography of the Arabidopsis Genome Is Organized in a Reduced Number of Linear Motifs of Chromatin States. The Plant Cell 26, 2351-2366.
Pubmed: Author and Title
CrossRef: Author and Title
Google Scholar: Author Only Title Only Author and Title

Simon, J.A., and Kingston, R.E. (2013). Occupying chromatin: polycomb mechanisms for getting to genomic targets, stopping transcriptional traffic, and staying put. Molecular cell 49, 808-824.
Pubmed: Author and Title
CrossRef: Author and Title
Google Scholar: Author Only Title Only Author and Title

Song, Y.H., Yoo, C.M., Hong, A.P., Kim, S.H., Jeong, H.J., Shin, S.Y., Kim, H.J., Yun, D.J., Lim, C.O., Bahk, J.D., Lee, S.Y., Nagao, R.T., Key, J.L., and Hong, J.C. (2008). DNA-binding study identifies C-box and hybrid C/G-box or C/A-box motifs as high-affinity binding sites for STF1 and LONG HYPOCOTYL5 proteins. Plant physiology 146, 1862-1877.
Pubmed: Author and Title
CrossRef: Author and Title
Google Scholar: Author Only Title Only Author and Title

Swiezewski, S., Liu, F., Magusin, A., and Dean, C. (2009). Cold-induced silencing by long antisense transcripts of an Arabidopsis Polycomb target. Nature 462, 799-802.
Pubmed: Author and Title
CrossRef: Author and Title
Google Scholar: Author Only Title Only Author and Title

Tavares, L., Dimitrova, E., Oxley, D., Webster, J., Poot, R., Demmers, J., Bezstarosti, K., Taylor, S., Ura, H., Koide, H., Wutz, A., Vidal, M., Elderkin, S., and Brockdorff, N. (2012). RYBP-PRC1 complexes mediate H2A ubiquitylation at polycomb target sites independently of PRC2 and H3K27me3. Cell 148, 664-678.
Pubmed: Author and Title
CrossRef: Author and Title
Google Scholar: Author Only Title Only Author and Title

Thomas-Chollier, M., Herrmann, C., Defrance, M., Sand, O., Thieffry, D., and van Helden, J. (2011). RSAT peak-motifs: motif analysis in full-size ChIP-seq datasets. Nucleic Acids Research 40, e31.
Pubmed: Author and Title
CrossRef: Author and Title
Google Scholar: Author Only Title Only Author and Title

Thomas-Chollier, M., Darbo, E., Herrmann, C., Defrance, M., Thieffry, D., and van Helden, J. (2012). A complete workflow for the analysis of full-size ChIP-seq (and similar) data sets using peak-motifs. Nature protocols 7, 1551-1568.
Pubmed: Author and Title
CrossRef: Author and Title
Google Scholar: Author Only Title Only Author and Title

Turck, F., Roudier, F., Farrona, S., Martin-Magniette, M.L., Guillaume, E., Buisine, N., Gagnot, S., Martienssen, R.A., Coupland, G., and Colot, V. (2007). Arabidopsis TFL2/LHP1 specifically associates with genes marked by trimethylation of histone H3 lysine 27. PLoS Genetics 3, e86.
Pubmed: Author and Title
CrossRef: Author and Title
Google Scholar: Author Only Title Only Author and Title

Vaquero-Sedas, M.I., Luo, C., and Vega-Palas, M.A. (2012). Analysis of the epigenetic status of telomeres by using ChIP-seq data. Nucleic Acids Research 40, e163.
Pubmed: Author and Title
CrossRef: Author and Title
Google Scholar: Author Only Title Only Author and Title

Vrbsky, J., Akimcheva, S., Watson, J.M., Turner, T.L., Daxinger, L., Vyskot, B., Aufsatz, W., and Riha, K. (2010). siRNA-mediated methylation of Arabidopsis telomeres. PLoS Genet 6, e1000986.
Pubmed: Author and Title
CrossRef: Author and Title
Google Scholar: Author Only Title Only Author and Title

Walter, M., Chaban, C., Schütze, K., Batistic, O., Weckermann, K., Näke, C., Blazevic, D., Grefen, C., Schumacher, K., Oecking, C., Harter, K., and Kudla, J. (2004). Visualization of protein interactions in living plant cells using bimolecular fluorescence complementation. Plant J 40, 428-438.
Pubmed: Author and Title
CrossRef: Author and Title
Google Scholar: Author Only Title Only Author and Title

Wan, F., Anderson, D.E., Barnitz, R.A., Snow, A., Bidere, N., Zheng, L., Hegde, V., Lam, L.T., Staudt, L.M., Levens, D., Deutsch, W.A., and Lenardo, M.J. (2007). Ribosomal protein S3: a KH domain subunit in NF-kappaB complexes that mediates selective gene regulation. Cell 131, 927-939.
Pubmed: Author and Title
CrossRef: Author and Title
Google Scholar: Author Only Title Only Author and Title

Yi, X., Du, Z., and Su, Z. (2013). PlantGSEA: a gene set enrichment analysis toolkit for plant community. Nucleic Acids Research 41, W98-103.
Pubmed: Author and Title
CrossRef: Author and Title
Google Scholar: Author Only Title Only Author and Title

Yilmaz, A., Mejia-Guerra, M.K., Kurz, K., Liang, X., Welch, L., and Grotewold, E. (2011). AGRIS: the Arabidopsis Gene Regulatory Information Server, an update. Nucleic Acids Research 39, D1118-1122.
Pubmed: Author and Title

CrossRef: Author and Title
Google Scholar: Author Only Title Only Author and Title

Zhang, H., He, H., Wang, X., Yang, X., Li, L., and Deng, X.W. (2011). Genome-wide mapping of the HY5-mediated gene networks in Arabidopsis that involve both transcriptional and post-transcriptional regulation. The Plant journal 65, 346-358.
Pubmed: Author and Title
CrossRef: Author and Title
Google Scholar: Author Only Title Only Author and Title

Zhang, H., Zeitz, M.J., Wang, H., Niu, B., Ge, S., Li, W., Cui, J., Wang, G., Qian, G., Higgins, M.J., Fan, X., Hoffman, A.R., and Hu, J.F. (2014). Long noncoding RNA-mediated intrachromosomal interactions promote imprinting at the Kcnq1 locus. The Journal of cell biology 204, 61-75.
Pubmed: Author and Title
CrossRef: Author and Title
Google Scholar: Author Only Title Only Author and Title

Zhang, X., Germann, S., Blus, B.J., Khorasanizadeh, S., Gaudin, V., and Jacobsen, S.E. (2007). The Arabidopsis LHP1 protein colocalizes with histone H3 Lys27 trimethylation. Nature Structural and Molecular Biology 14, 869-871.
Pubmed: Author and Title
CrossRef: Author and Title
Google Scholar: Author Only Title Only Author and Title

Zhang, Y., Liu, T., Meyer, C.A., Eeckhoute, J., Johnson, D.S., Bernstein, B.E., Nusbaum, C., Myers, R.M., Brown, M., Li, W., and Liu, X.S. (2008). Model-based analysis of ChIP-Seq (MACS). Genome Biology 9, R137.
Pubmed: Author and Title
CrossRef: Author and Title
Google Scholar: Author Only Title Only Author and Title

Zhou, J., Wang, X., He, K., Charron, J.B., Elling, A.A., and Deng, X.W. (2010). Genome-wide profiling of histone H3 lysine 9 acetylation and dimethylation in Arabidopsis reveals correlation between multiple histone marks and gene expression. Plant Molecular Biology 72, 585-595.
Pubmed: Author and Title
CrossRef: Author and Title
Google Scholar: Author Only Title Only Author and Title

Zhou, Y., Hartwig, B., Velikkakam James, G., Schneeberger, K., and Turck, F. (2015). Complementary activities of TELOMERE REPEAT BINDING proteins and Polycomb Group complexes in transcriptional regulation of target genes. The Plant Cell.
Pubmed: Author and Title
CrossRef: Author and Title
Google Scholar: Author Only Title Only Author and Title

Zilberman, D., Coleman-Derr, D., Ballinger, T., and Henikoff, S. (2008). Histone H2A.Z and DNA methylation are mutually antagonistic chromatin marks. Nature 456, 125-129.
Pubmed: Author and Title
CrossRef: Author and Title
Google Scholar: Author Only Title Only Author and Title

A

Reads	Total Number	Uniquely mapped
LHP1 IP rep1	49 337 103	22 535 892
LHP1 INPUT rep1	44 858 478	26 075 751
LHP1 IP rep2	51 830 947	17 161 379
LHP1 INPUT rep2	47 477 630	17 480 420
LIF2 IP rep1	46 292 522	17 954 623
LIF2 INPUT rep1	50 345 677	21 072 356
LIF2 IP rep2	47 453 337	12 953 623
LIF2 INPUT rep2	47 070 104	18 201 752

B

	Covered nucleotides	Nbre regions covered
LIF2 rep1	5034884	1750
LIF2 rep2	6913458	2442
Intersect beween LIF2 rep1 & rep2	3937459	1457
LHP1 rep1	23794547	4901
LHP1 rep2	23881395	5095
Intersect beween LHP1 rep1 & rep2	21988263	4844

C

Overlap between replicates	%
In nucleotides	
related to LIF2 rep1	78.20
related to LIF2 rep2	56.95
related to LHP1 rep1	92.41
related to LHP1 rep2	92.07
In numbrer of regions	
related to LIF2 rep1	83.26
related to LIF2 rep2	59.66
related to LHP1 rep1	98.84
related to LHP1 rep2	95.07

D

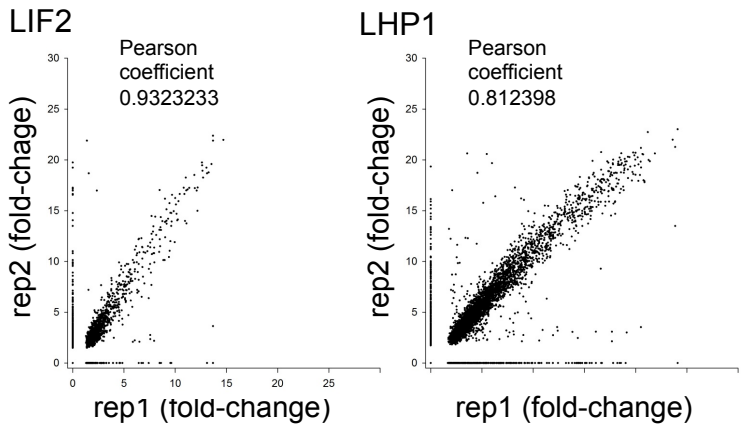

E

AGI		Annotation	LHP1 rep1	LHP1 rep2	LIF2 rep1	LIF2 rep2
AT5G60390	EF1	CDS	0	0	0	0
AT5G15840	CO	CDS	0	0	0	0
AT3G15210	ERF4	CDS	0	0	12.09	16.97
AT1G19180	JAZ1	5'UTR	0	0	7.97	9.9
AT1G32640	MYC2	CDS	0	0	4.05	5.7
AT1G52890	NAC19	CDS	7.68	9.08	2.86	2.21
AT5G45830	DOG1	CDS	11.59	11.2	0	0
AT1G47860		TE	4.41	5.18	3.65	4.03
AT1G21300		TE	8.33	11.47	0	0
AT4G31877	miR156C	ncRNA	15.71	15.98	0	0

F

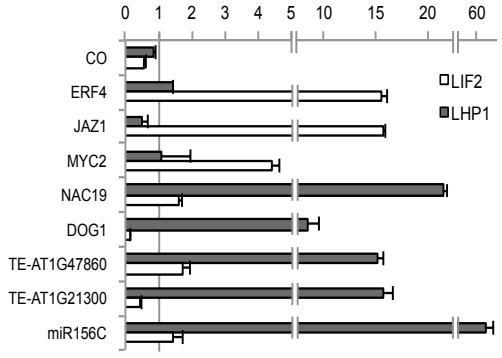

Supplemental Figure 1: ChIP-seq experiments.
(**A**) Read counts and mapping in the two ChIP-seq biological replicates.
(**B**) Comparisons between replicates.
(**C**) Overlaps between replicates.
(**D**) MACS peak fold-change correlations between ChIP-seq replicates.
(**E**) Fold-changes in the two ChIP-seq biological replicates of selected target regions.
(**F**) Confirmation by ChIP-QPCR at targets identified by ChIP-seq. Protein enrichments were relative to input and the internal reference gene, *EF1α*. The values correspond to the mean of two biological replicates and three technical replicates for each ±SE.

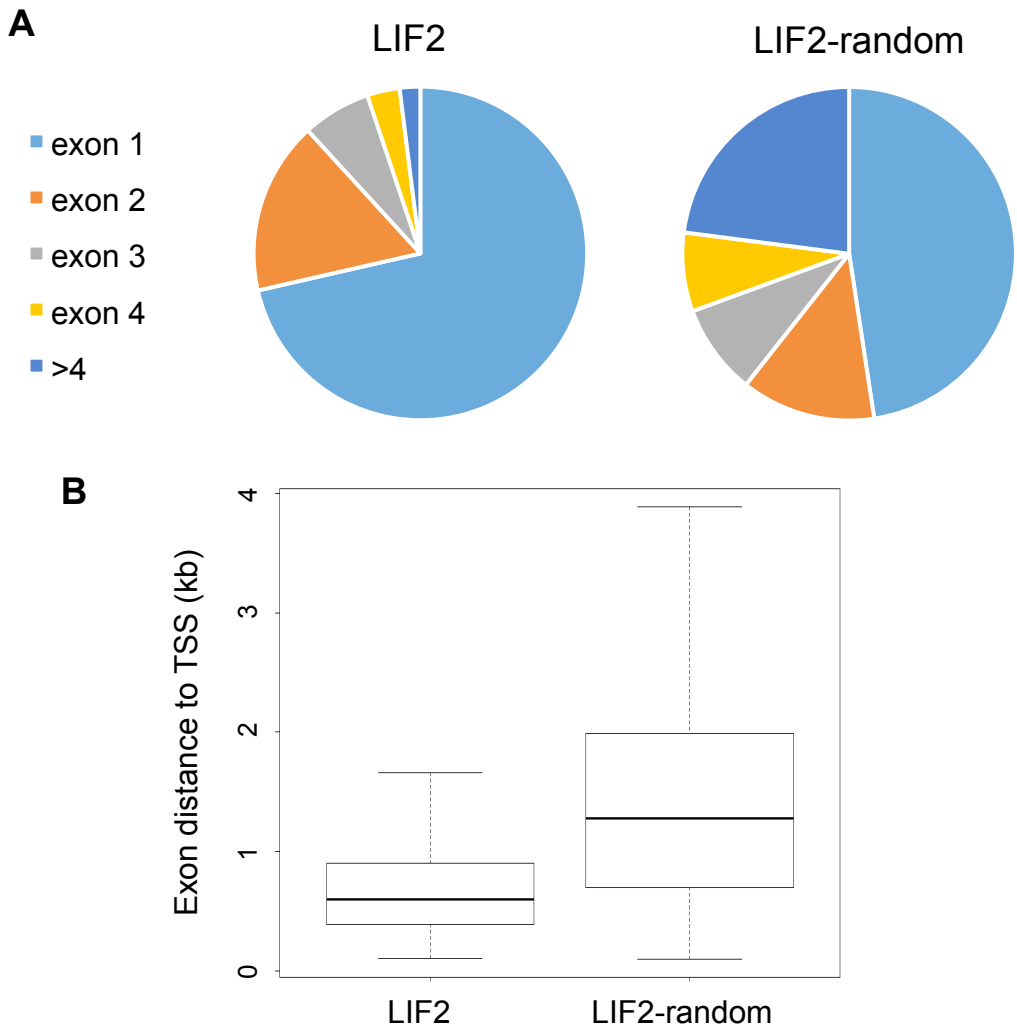

Supplemental Figure 2: Exon distributions of LIF2 ERs.
(**A**) Exon number distribution of LIF2 ERs and comparisons with the randomly shuffled control regions.
(**B**) Distance to TSS of the LIF2-bound exons and comparisons with the randomly shuffled control regions.

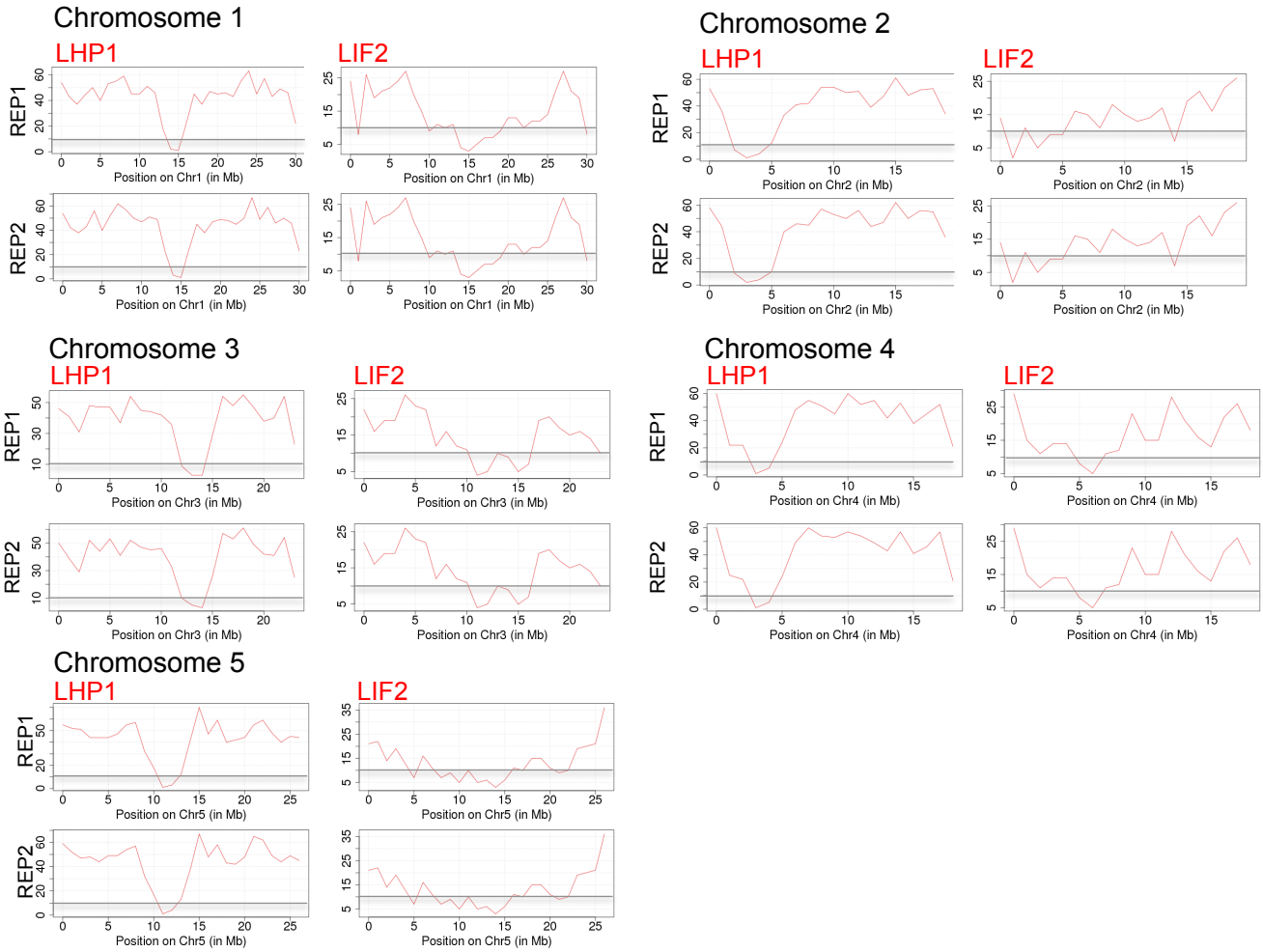

Supplemental Figure 3: Distributions of the sums of the summits in 1-Mb windows. For the two biological replicates, LHP1 and LIF2 distributions on the five chromosomes were compared by plotting the sums of their summits in 1-Mb windows.

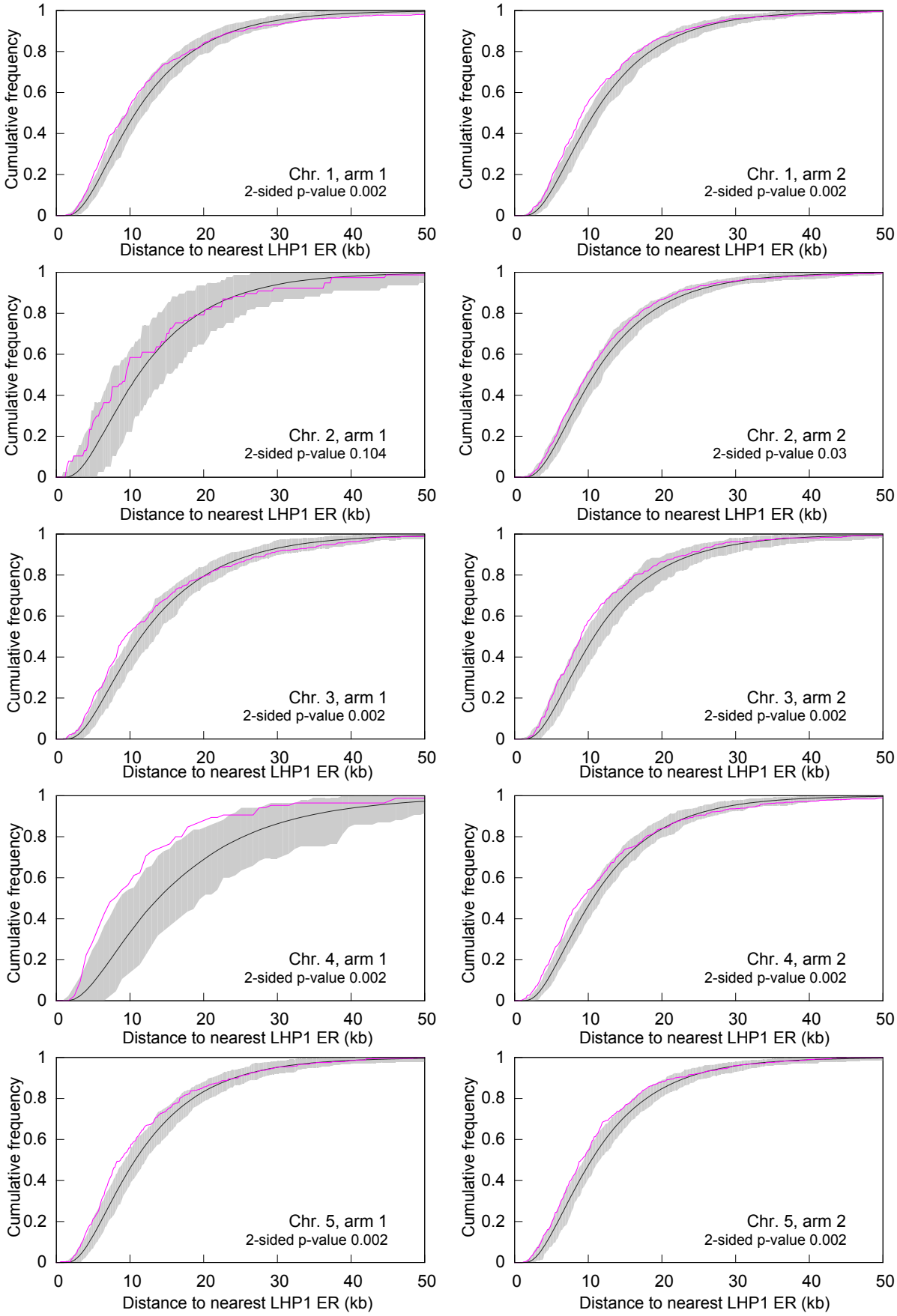

Supplemental Figure 4: Cumulative distribution of the distance to the nearest LHP1 summit. Pink: observed distribution; black: average distribution under the random model; grey: 95% envelope under the random model. Arm 1 of chromosome 2 and arm 1 of chromosome 4 bear the NOR and the knob, respectively, which introduce spatial constraints.

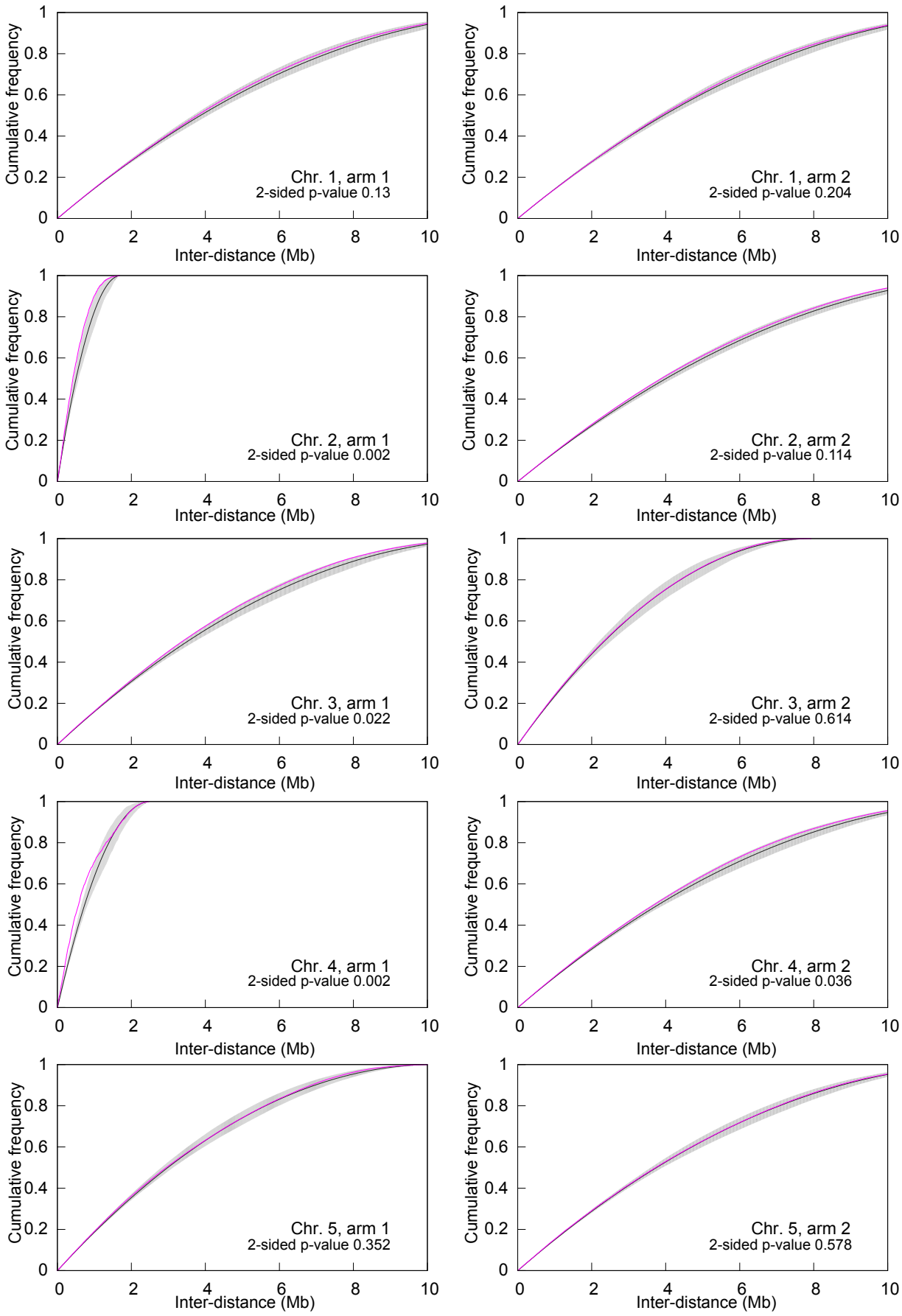

Supplemental Figure 5: Cumulative distribution of LHP1 summit inter-distances. Pink: observed distribution; black: average distribution under the random model; grey: 95% envelope under the random model. Arm 1 of chromosome 2 and arm 1 of chromosome 4 bear the NOR and the knob, respectively, which introduce spatial constraints.

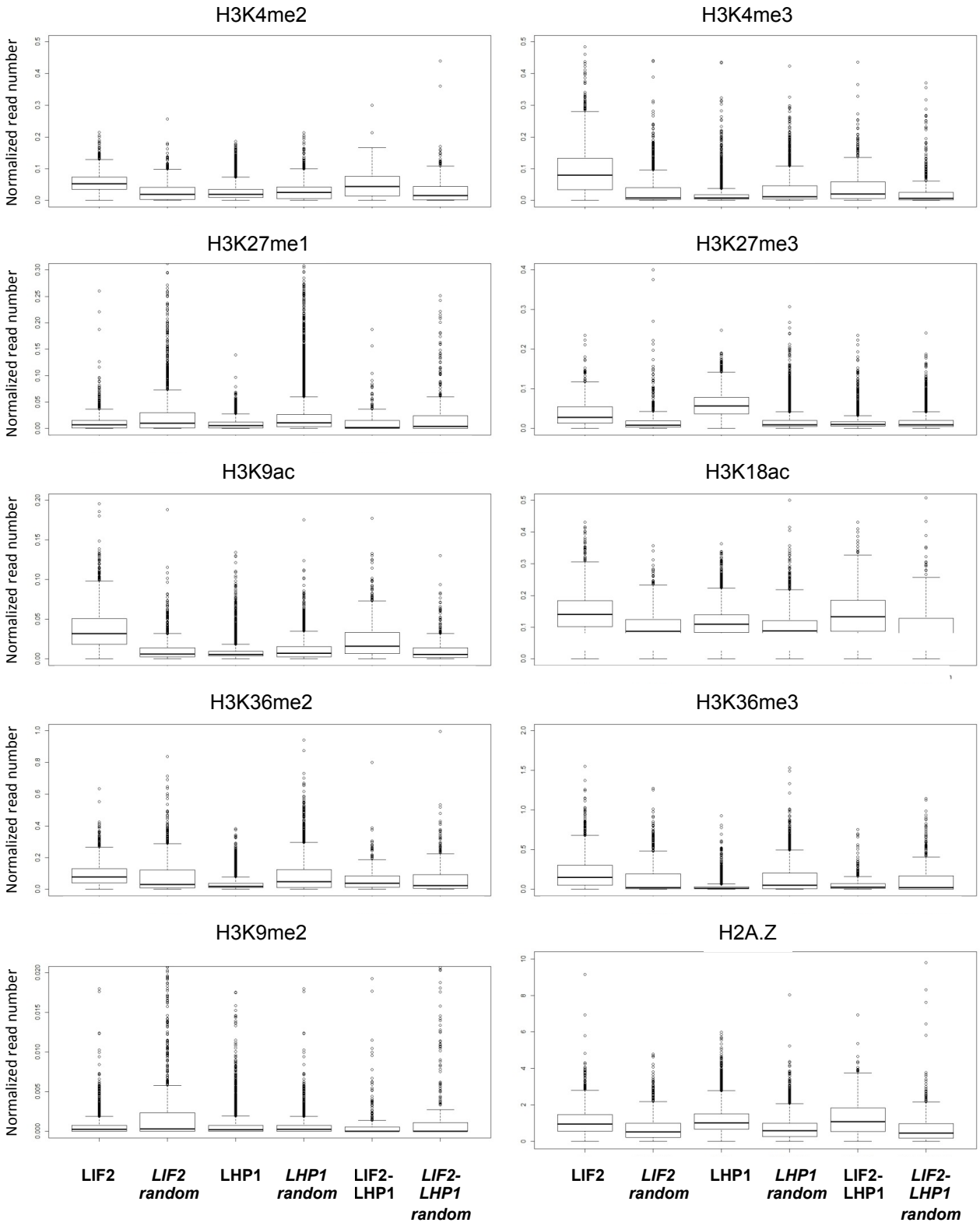

Supplemental Figure 6: Post-translational histone modifications and their distributions in LIF2 ERs, LHP1 ERs and LIF2-LHP1 IRs.

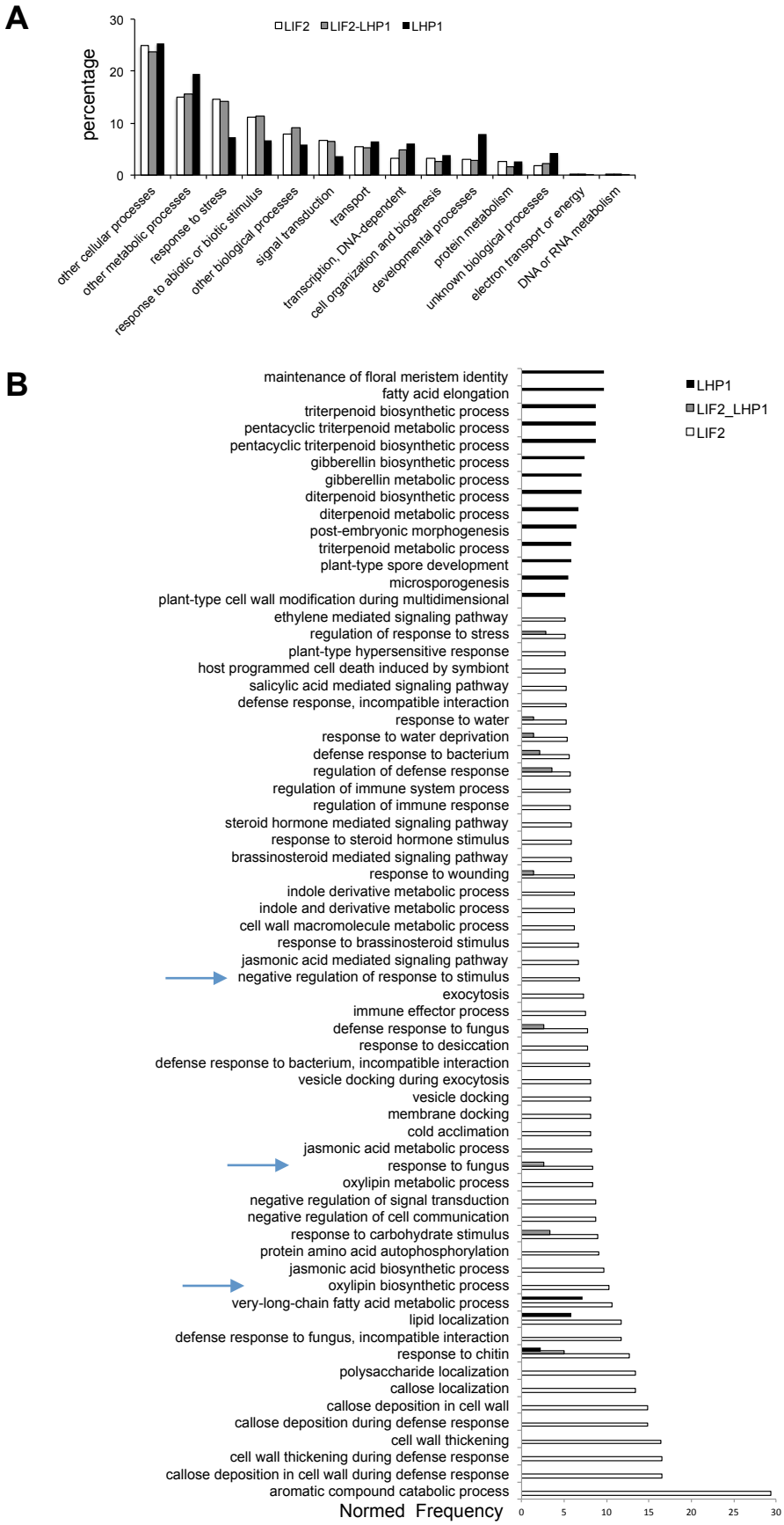

Supplemental Figure 7: GO term analysis of the target loci of LIF2 and LHP1.
(**A**) Functional categorization of the LIF2 ERs, LHP1 ERs and LIF2-LHP1 IRs (TAIR GO toolkit).
(**B**) Normed frequencies (NF) of the GO terms in the biological process categories with an over 4-fold enriched NF in at least one of the input lists (*i.e.,* LIF2 target genes, LHP1 target genes, genes of LIF2-LHP1 IRs) were compiled using AgriGO toolkit. Arrows: GO terms related to JA.

A

LIF2-LHP1 targets		
Set-90	Set-64	Set-21
AT1G03850	AT1G02390	AT1G21010
AT1G03870	AT1G02400	AT1G21550
AT1G09950	AT1G02920	AT1G58420
AT1G12110	AT1G12090	AT1G61890
AT1G22570	AT1G13260	AT1G65390
AT1G22710	AT1G17420	AT1G69900
AT1G24530	AT1G18570	AT1G72520
AT1G25440	AT1G21910	AT1G78850
AT1G25550	AT1G24140	AT2G04495
AT1G26250	AT1G25400	AT2G43060
AT1G29280	AT1G28370	AT4G18950
AT1G34245	AT1G30720	AT4G23170
AT1G35560	AT1G33610	AT4G30280
AT1G37130	AT1G33760	AT4G39640
AT1G44350	AT1G35140	AT5G11550
AT1G52890	AT1G35210	AT5G19230
AT1G54740	AT1G36060	AT5G20230
AT1G58270	AT1G53170	AT5G59820
AT1G68520	AT1G61260	AT5G61600
AT1G70170	AT1G66090	AT5G64260
AT1G71880	AT1G66180	AT5G66650
AT1G72430	AT1G77640	
AT1G75500	AT1G80840	
AT1G75710	AT2G05520	
AT1G80450	AT2G18690	
AT2G02680	AT2G22500	
AT2G05380	AT2G24600	
AT2G19810	AT2G25450	
AT2G22470	AT2G26560	
AT2G32030	AT2G30362	
AT2G32140	AT2G35930	
AT2G36950	AT2G44840	
AT2G40750	AT3G01290	
AT2G41100	AT3G10300	
AT2G42350	AT3G10720	
AT2G45400	AT3G22160	
AT2G46160	AT3G48520	
AT2G47485	AT3G49120	
AT2G48030	AT3G50260	
AT3G07350	AT3G50480	
AT3G15500	AT3G52400	
AT3G18950	AT3G52450	
AT3G22910	AT3G56400	
AT3G23030	AT3G56710	
AT3G23250	AT4G00360	
AT3G28910	AT4G01950	
AT3G44720	AT4G02330	
AT3G46090	AT4G08950	
AT3G48650	AT4G20000	
AT3G49780	AT4G22690	
AT3G50740	AT4G25470	
AT3G52470	AT4G30270	
AT3G60520	AT4G32800	
AT3G62690	AT5G04340	
AT4G00730	AT5G17350	
AT4G16780	AT5G21960	
AT4G16820	AT5G25250	
AT4G17460	AT5G26920	
AT4G23880	AT5G35735	
AT4G25480	AT5G42380	
AT4G32290	AT5G43760	
AT4G32480	AT5G47220	
AT4G34380	AT5G54720	
AT4G36010	AT5G64120	
AT4G36670		
AT4G36900		
AT4G37540		
AT4G38620		
AT4G39950		
AT5G06300		
AT5G07080		
AT5G09440		
AT5G12340		
AT5G14730		
AT5G14920		
AT5G24930		
AT5G26340		
AT5G37540		
AT5G40720		
AT5G41810		
AT5G46295		
AT5G49280		
AT5G49520		
AT5G49700		
AT5G54710		
AT5G62020		
AT5G62470		
AT5G64750		
AT5G67430		
AT5G67450		

B

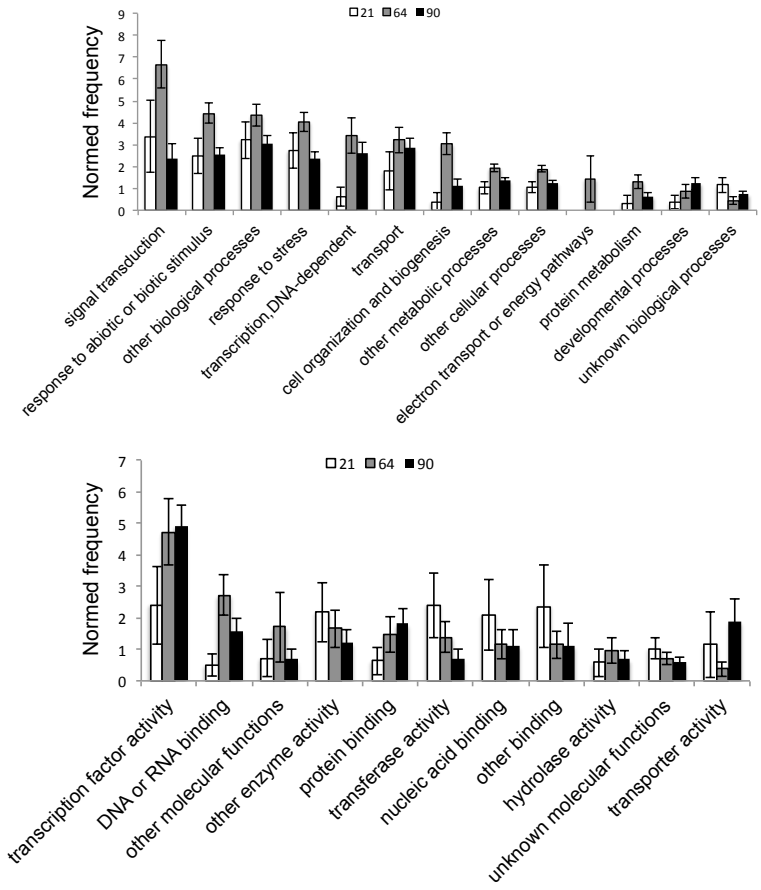

C

Biological process	Description	NO. Genes in Overlap	Tot. NO. Genes in GO	p-value	FDR
Set-21					
Response to wounding	GO:0009611	6	340	1.34e-07	7.93e-05
Oxylipin metabolic process	GO:0031407	5	167	1.35e-07	7.93e-05
JA metabolic process	GO:0009694	5	159	1.07e-07	7.93e-05
Set-64					
Response to chitin	GO:0010200	22	421	3.33e-24	1.43e-20
Reg. of innate immune response	GO:0045088	20	415	2.57e-21	3.3e-18
Reg. of immune system process	GO:0002682	20	419	3.08e-21	3.3e-18
Set-90					
Response to chemical stimulus	GO:0042221	37	953	1.78e-10	7.95e-07
Response to stimulus	GO:0050896	45	6222	3.09e-09	4.6e-06
Response to organic substance	GO:0010033	29	2739	2.46e-09	4.6e-06

D

Expression profiles	Set-90	Set-64	Set-21
No change in transcriptomes	54 (60.0%)	26 (40.6%)	7 (33.3%)
Deregulation in *lif2*	19	31	9
Deregulation in *lhp1*	28 (31.1%)	22	11
Deregulation in *lif2 & lhp1*	11	15	6
Down in *lif2*	14	29 (45.3%)	8
Up in *lif2*	5	0	1
Down in *lhp1*	7	9	4
Up in *lhp1*	18	10	4
Down in *lif2 & lhp1*	2	7	3
Up in *lif2 & lhp1*	3	0	1

Supplemental Figure 8: Analyses of the LIF2-LHP1 IRs with binding alterations in the mutant backgrounds.
(**A**) Lists of the three sets of genes.
(**B-C**) GO analyses using BAR and Plant GSEA toolkits, respectively.
(**D**) Expression profiles of the gene sets. Percentages related to the number of genes in the Set were calculated for the largest classes.

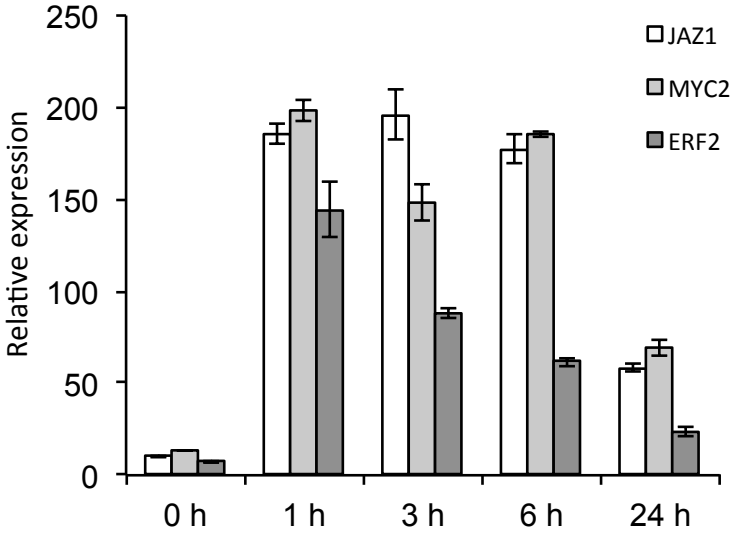

Supplemental Figure 9: Expression kinetics of JA-induced marker genes in response to MeJA treatment in wild-type plants.
Two-week-old seedlings were treated with JA for 1 to 24 hours and *JAZ1*, *MYC2* and *ERF2* expression was recorded. *EF1* was used as reference gene.

Tandem duplications (T-Clusters)	Chromosome 4	Whole genome
T-Clusters	248	1564
T-Cluster genes	681	4176
Average T-Cluster size (gene number)	2.75	2.67
T-Clusters & LHP1 targets genes	132	861
% of T-Cluster genes targeted by LHP1	19.4	20.6
% of LHP1 target genes in T-Clusters	23.8	23.1
LHP1 target genes in T-Clusters (with no unannotated genes in the cluster)	n.d.	848
Clusters with 1 LHP1 target gene per cluster	n.d.	484
Clusters with 2 LHP1 target gene per cluster	n.d.	138
Clusters with 3 LHP1 target gene per cluster	n.d.	20
Clusters with 4 LHP1 target gene per cluster	n.d.	7
% of LHP1 targeted genes in T-clusters that have multiple LHP1 targets	n.d.	9.6%

Supplemental Table 1 : Tandem duplications and LHP1 target genes.
n.d. non determinded.

	LIF2		LIF2-LHP1	
	Normed Frequency	p-value	Normed Frequency	p-value
Biological process				
signal transduction	3.34	1.753e-50	2.82	2.213e-11
other biological processes	3.22	1.652e-87	3.27	8.384e-29
response to abiotic or biotic stimulus	3	1.399e-78	2.7	2.662e-19
response to stress	2.98	2.398e-87	2.67	5.353e-21
transport	2.32	2.349e-36	2.22	5.928e-11
transcription,DNA-dependent	1.71	8.047e-10	2.15	1.356e-07
other cellular processes	1.35	1.633e-24	1.24	4.149e-05
other metabolic processes	1.34	3.208e-20	1.32	6.090e-07
cell organization and biogenesis	1.2	5.091e-03	0.97	0.079
electron transport or energy pathways	1.19	0.060	0.33	0.043
developmental processes	1.13	0.013	1.04	0.071
protein metabolism	1.05	0.026	0.63	1.059e-03
unknown biological processes	0.58	1.403e-18	0.68	1.004e-04
DNA or RNA metabolism	0.27	6.744e-06	0.12	2.346e-03
Molecular function				
transcription factor activity	2.39	3.730e-18	3.7	2.739e-17
DNA or RNA binding	1.16	0.011	1.39	6.066e-03
receptor binding or activity	1.43	0.100	1.31	0.255
protein binding	1.9	1.958e-13	1.29	0.031
other enzyme activity	1.2	0.033	1.25	0.082
other molecular functions	1.2	3.401e-03	1.25	0.022
transporter activity	1.12	0.050	1.16	0.097
other binding	1.17	6.249e-04	1.12	0.032
transferase activity	1.52	4.876e-07	1.05	0.078
nucleic acid binding	0.53	1.859e-04	0.72	0.068
unknown molecular functions	0.66	3.823e-12	0.71	3.973e-04
hydrolase activity	1.01	0.045	0.7	0.022
kinase activity	1.83	5.319e-07	0.68	0.070
nucleotide binding	1.15	0.011	0.64	9.169e-03
structural molecule activity	0.52	0.016	0.63	0.154

Supplemental Table 2: GO term analysis of the genes present in LIF2 ERs and LIF2-LHP1 IRs using the Plant Functional Genomics (BAR) classification Superviewer program.

TF family	Nbr Genes	Total in family	p-value	FDR
LIF2				
AP2-EREBP	24	138	1.57e-11	1.79e-08
WRKY	12	72	2.82e-06	1.07e-03
LIF2_LHP1				
AP2-EREBP	17	138	2.72e-14	1.11e-11
C2C2-CO-Like	4	30	1.97e-04	0.0202
C2H2	8	211	6.24e-04	0.0488
WRKY	6	72	5.63e-05	7.68e-03
LHP1				
C2H2	34	211	1,00E-04	0.0146
BASIC HELIX-LOOP-HELIX (bHLH)	33	162	1.94e-06	5.27e-04
BHLH	33	161	1.73e-06	5.27e-04
MADS	31	109	7.36e-09	4.66e-06
MADS-BOX	31	108	6.13e-09	4.66e-06
HOMEOBOX	29	91	2.66e-09	4.66e-06
MYB	27	131	1.34e-05	2.82e-03
MYB3R- and R2R3- TYPE MYB-encoding genes	27	132	1.5e-05	2.86e-03
NAC	19	96	3.76e-04	0.0434
WRKY	18	72	4.29e-05	6.79e-03
ZINC FINGER-HOMEOBOX - ZHD subfamily	7	14	3.88e-04	0.0434

Supplemental Table 3: Enrichments of LIF2 and LHP1 targets in specific transcription factor families using the PlantGSEA resource.

TF	Genes targeted	Total genomic targets	p-value	FDR	Genes targeted by TF in ERs
LIF2					
AGL15 (MADS box)	7	22	9.89e-06	1.69e-04	AT1G02400 AT1G14920 AT4G25470 AT2G45830 AT4G38680 AT1G68840 AT1G13260
AP2 (AP2/EREBP)	18	165	2.87e-06	5.73e-05	AT1G11050 AT1G13260 AT1G22530 AT1G23390 AT1G71030 AT3G55980 AT4G00730 AT4G01250 AT4G02540 AT4G08950 AT4G16490 AT4G20260 AT4G25480 AT4G26690 AT4G29190 AT5G19140 AT5G20250 AT5G49360
PIF1 (AtbHLH15)	22	189	8.38e-08	2.51e-06	AT1G25550 AT1G28330 AT1G52890 AT1G56220 AT1G60190 AT1G68670 AT2G01570 AT2G16660 AT2G27500 AT2G45820 AT2G46710 AT3G02550 AT3G04730 AT3G12920 AT3G24050 AT3G24503 AT3G25870 AT4G17460 AT5G24930 AT5G54380 AT5G64260 AT5G65430
HY5 (bZIP)	61	221	6.37e-37	7.64e-35	AT1G07135 AT1G09070 AT1G17420 AT1G18300 AT1G18570 AT1G20510 AT1G21910 AT1G24140 AT1G24530 AT1G53170 AT1G56660 AT1G60190 AT1G61340 AT1G61890 AT1G66160 AT1G68840 AT1G69760 AT1G73500 AT1G77640 AT1G78850 AT2G22500 AT2G25460 AT2G27660 AT2G30040 AT2G33580 AT2G35290 AT2G35930 AT2G39650 AT2G41100 AT2G41640 AT3G06080 AT3G14440 AT3G25250 AT3G46080 AT3G48520 AT3G52400 AT3G54810 AT3G55980 AT3G56880 AT3G62260 AT3G62720 AT4G08950 AT4G17500 AT4G25490 AT4G27310 AT4G29780 AT4G32800 AT4G33920 AT4G34150 AT4G36670 AT5G01100 AT5G43890 AT5G45110 AT5G45340 AT5G49280 AT5G49520 AT5G52020 AT5G59550 AT5G62020 AT5G62520 AT5G66650
LIF2_LHP1					
AGL15 (MADS box)	4	22	6.71e-05	7.64e-04	AT1G02400 AT1G13260 AT2G45830 AT4G25470
AP2 (AP2/EREBP)	6	165	3.61e-03	0.0274	AT4G00730 AT4G37540 AT4G25480 AT4G08950 AT5G54470 AT1G13260
PIF1 (AtbHLH15)	6	189	6.79e-03	0.0441	AT1G03850 AT1G25550 AT1G52890 AT4G17460 AT5G24930 AT5G64260
HY5 (bZIP)	30	221	1.75e-25	7.97e-24	AT1G17420 AT1G18570 AT1G21910 AT1G24140 AT1G24530 AT1G25400 AT1G53170 AT1G61890 AT1G77640 AT1G78850 AT2G22500 AT2G27660 AT2G35290 AT2G35930 AT2G37430 AT2G41100 AT3G25250 AT3G46080 AT3G48520 AT3G52400 AT4G08950 AT4G32800 AT4G36670 AT5G43890 AT5G49280 AT5G49520 AT5G52020 AT5G59820 AT5G62020 AT5G66650
LHP1					
AP2 (AP2/EREBP)	30	165	3.73e-05	1.68e-03	AT2G16760 AT2G14210 AT5G54470 AT1G71050 AT4G00730 AT4G04630 AT5G67180 AT5G07030 AT3G58780 AT4G36870 AT2G40435 AT5G15310 AT4G13210 AT2G18550 AT2G43620 AT2G45660 AT1G35910 AT1G70560 AT4G18960 AT5G64870 AT4G37540 AT5G13790 AT1G73590 AT5G67060 AT1G13260 AT1G35730 AT3G55710 AT2G42830 AT4G08950 AT4G24050
HY5 (bZIP)	42	221	4.27e-07	5.86e-05	AT1G24530 AT5G52020 AT5G25810 AT1G78990 AT1G17420 AT3G52400 AT2G47460 AT1G61890 AT5G23010 AT4G27250 AT1G02810 AT2G22500 AT5G49520 AT5G57510 AT1G16850 AT4G36670 AT3G55120 AT2G37430 AT1G53170 AT5G59820 AT5G66650 AT1G32450 AT5G44120 AT5G42800 AT2G28630 AT3G48520 AT5G62490 AT5G24140 AT5G59780 AT2G15020 AT3G21720 AT5G49280 AT1G17380 AT5G10100 AT4G08950 AT4G05100 AT2G41100 AT3G22830 AT5G62020 AT1G78850 AT1G12950 AT5G13930
SEP3 (MADS box)	11	15	5.4e-07	5.86e-05	AT3G54340 AT2G22540 AT3G58780 AT3G02310 AT2G45660 AT4G18960 AT5G13790 AT2G03710 AT4G24540 AT2G42830 AT5G15800

Supplemental Table 4: LIF2 and LHP1 targets are also bound by specific transcription factors.
The PlantGSEA and AGRIS toolkits were used.

Segment Name	Unique sequence occurrences	Total occurrence	Expected unique sequence	Expected occurrences	Rank	Score
ACGTGGCA word						
Distal Promoter	598	621	497.582	503.982	1175	109.93
Proximal Promoter	414	431	353.216	358.329	1251	65.7371
Core Promoter	172	174	141.099	152.113	539	34.061
5'UTR	26	26	15.5612	16.4062	3156	13.3462
Intron	48	48	38.8425	40.5848	21162	10.161
3'UTR	26	27	21.3065	22	14830	5.1762
Genome-wide	5	1265	5	1020.69	2410	0
AAACCCTA word						
Intron	764	802	652.752	686.061	672	120.231
5'UTR	911	952	825.505	908.536	26	89.7771
Distal Promoter	3116	3674	3041.64	3238.08	2631	75.2602
Core Promoter	639	658	568.781	618.048	51	74.3858
Proximal Promoter	1606	1779	1540.73	1598.78	1209	66.6328
3'UTR	91	92	75.7094	78.332	2976	16.7401
Genome-wide	5	11340	5	9887.71	55	0

Supplemental Table 5: Occurrences of the two identified DNA words.
The word frequency calculation was performed in non-coding segments of the *A. thaliana* genome, using the Arabidopsis *cis*-regulatory element database (http://arabidopsis.med.ohio-state.edu/AtcisDB/).

GO term	Description	Normed frequency	p-value	FDR
lhp1 LIF2 depleted				
Biological process				
GO:0052542	callose deposition during defense response	31,5	1.4e-06	2.4e-05
GO:0033037	polysaccharide localization	28,5	2.2e-06	3.3e-05
GO:0052545	callose localization	28,5	2.2e-06	3.3e-05
GO:0010200	response to chitin	24,5	2.1e-31	5.0e-29
GO:0009631	cold acclimation	20,6	8.7e-06	0.00013
GO:0002252	immune effector process	19,3	1.2e-05	0.00016
GO:0031408	oxylipin biosynthetic process	18,7	1.3e-05	0.00018
GO:0009867	jasmonic acid mediated signaling pathway	17,1	4.1e-07	7.6e-06
GO:0009743	response to carbohydrate stimulus	16,9	1.5e-29	2.4e-27
GO:0031407	oxylipin metabolic process	15,3	3.2e-05	0.00041
GO:0002682	regulation of immune system process	14,6	4.0e-05	0.00049
GO:0050776	regulation of immune response	14,6	4.0e-05	0.00049
GO:0042434	indole derivative metabolic process	13,5	9.7e-06	0.00014
GO:0042430	indole and derivative metabolic process	13,5	9.7e-06	0.00014
GO:0050832	defense response to fungus	13,3	4.1e-10	1.4e-08
GO:0009873	ethylene mediated signaling pathway	12,9	4.3e-07	7.7e-06
GO:0031347	regulation of defense response	12,7	2.6e-06	3.9e-05
GO:0080134	regulation of response to stress	11,5	9.6e-07	1.7e-05
GO:0009620	response to fungus	11,3	2.0e-11	1.1e-09
GO:0000160	two-component signal transduction system (phosphorelay)	10,4	2.0e-06	3.2e-05
GO:0009611	response to wounding	10,3	3.8e-12	2.3e-10
GO:0042742	defense response to bacterium	10,1	9.0e-11	4.3e-09
GO:0009415	response to water	10,0	8.4e-14	7.3e-12
GO:0009414	response to water deprivation	9,9	3.8e-13	3.0e-11
GO:0019760	glucosinolate metabolic process	9,6	0.00024	0.0026
GO:0016143	S-glycoside metabolic process	9,6	0.00024	0.0026
GO:0019757	glycosinolate metabolic process	9,6	0.00024	0.0026
GO:0048585	negative regulation of response to stimulus	8,7	9.5e-05	0.0011
GO:0006955	immune response	8,5	5.5e-16	6.2e-14
GO:0002376	immune system process	8,4	5.9e-16	6.2e-14
GO:0045087	innate immune response	8,3	1.2e-14	1.2e-12
GO:0009642	response to light intensity	8,0	0.00015	0.0018
GO:0009617	response to bacterium	7,7	8.6e-10	2.7e-08
GO:0009723	response to ethylene stimulus	7,2	2.4e-07	4.9e-06
GO:0006952	defense response	7,2	9.6e-25	1.3e-22
Molecular function				
GO:0016564	transcription repressor activity	17,1	9.0e-09	8.9e-07
lif2 LHP1 depleted				
Biological process				
GO:0010876	lipid localization	16,7	5.6e-13	3.6e-11
GO:0010076	maintenance of floral meristem identity	16,7	1.2e-05	0.00037
GO:0046087	cytidine metabolic process	16,7	1.2e-05	0.00037
GO:0006216	cytidine catabolic process	16,7	1.2e-05	0.00037
GO:0009972	cytidine deamination	16,7	1.2e-05	0.00037
GO:0046135	pyrimidine nucleoside catabolic process	15,0	1.8e-05	0.00053
GO:0046133	pyrimidine ribonucleoside catabolic process	15,0	1.8e-05	0.00053
GO:0010022	meristem determinacy	13,9	0.00013	0.0027
GO:0009164	nucleoside catabolic process	13,6	2.8e-05	0.00075
GO:0042454	ribonucleoside catabolic process	13,6	2.8e-05	0.00075
GO:0034656	nucleobase, nucleoside and nucleotide catabolic process	12,5	4.0e-05	0.001
GO:0034655	nucleobase, nucleoside, nucleotide and nucleic acid catabolic process	12,5	4.0e-05	0.001
GO:0045962	positive regulation of development, heterochronic	12,5	0.00018	0.0038
GO:0046131	pyrimidine ribonucleoside metabolic process	10,7	7.8e-05	0.0019
GO:0006213	pyrimidine nucleoside metabolic process	10,0	0.00011	0.0023
GO:0009886	post-embryonic morphogenesis	9,3	2.1e-08	9.7e-07
GO:0045596	negative regulation of cell differentiation	8,1	8.1e-07	3.2e-05
GO:0065001	specification of axis polarity	7,9	9.1e-05	0.0021
GO:0016145	S-glycoside catabolic process	7,9	0.0003	0.006
GO:0019759	glycosinolate catabolic process	7,9	0.0003	0.006
GO:0019762	glucosinolate catabolic process	7,9	0.0003	0.006
GO:0010089	xylem development	7,8	0.001	0.017
GO:0016139	glycoside catabolic process	7,5	0.00038	0.0073
GO:0010074	maintenance of meristem identity	7,4	4.4e-05	0.0011
GO:0048440	carpel development	7,4	3.6e-11	2.0e-09
GO:0009943	adaxial/abaxial axis specification	7,3	0.00014	0.0031
GO:0019827	stem cell maintenance	7,3	1.7e-05	0.0005
GO:0048864	stem cell development	7,3	1.7e-05	0.0005
GO:0009944	polarity specification of adaxial/abaxial axis	7,1	0.00048	0.0088
GO:0006722	triterpenoid metabolic process	7,1	0.00048	0.0088
GO:0048467	gynoecium development	7,0	2.7e-11	1.5e-09
GO:0048863	stem cell differentiation	7,0	2.1e-05	0.00059

Supplemental Table 6: GO term analysis of LIF2 or LHP1 depleted regions in the mutant backgrounds (AgriGO).
Lists of GO terms with NF ≥7.

Primer	Sequence (5' to 3')	Application
3HA-1	ACACACACTGCAGGGGTTAATTAACATCTTTTACCC	Cloning
3HA-2	CGGAATCTAGAGTCGACGCTGCACTGAGCAGCGTAA	Cloning
3HA-2	CCGGATATCGTCGACGGGTTAATTAACATCTTTTACCC	Cloning
3HA-2	CGGGATATCTTACTCGAGGCACTGAGCAGCGTAATCTGG	Cloning
Nost-1	CCTAAGGTACCGAATTTCCCCGATCGTTCA	Cloning
Nost-2	CGGGAATTCCCGATCTAGTAACATA	Cloning
AD379-28	TACGCAGCTGTTGTAATCCAA	Cloning
AD379-29	CATTATCCTGCAGGTCTGACATCTGGTCATC	Cloning
AD379-30	TTCCCCTCGAGATGTCAGACGCAAGAGATAA	Cloning
AD379-32	TTGAAAGTTGAAACAAAATCAATCA	Cloning
JAZ1_F	AGCTTCACTTCACCGGTTCTTGGA	qRT-PCR
JAZ1_R	TCTTGTCTTGAAGCAACGTCGTCA	qRT-PCR
JAZ9_F	TGCTGTCGAAGAACGAGGGT	qRT-PCR
JAZ9_R	CTTCCCCCATTCTCTAGCTGC	qRT-PCR
LOX3_F	CGGATAGAGAAAGAGATTGAGAAAAGGAAC	qRT-PCR
LOX3_R	GGTACACCTCTACACGTAACACCAGGC	qRT-PCR
MYC2_F	GCCGAAGGAATACACGCAAT	qRT-PCR
MYC2_R	CGGGTTGTGAACGGGCTA	qRT-PCR
VSP2_F	TAGGCTTCAATATGAGATGCTTCCAGT	qRT-PCR
VSP2_R	ACCGTTGGAAATTGTGGAAGAATG	qRT-PCR
JAZ6_A_F	GTCTGCTCAGCCGGTACTTG	qChIP/qRT-PCR
JAZ6_A_R	TTCGAGCCAACCCCATATTA	qChIP/qRT-PCR
CO_F	AAC AAT GAC CGA TCC AGA GAA	qChIP/qRT-PCR
CO_R	CCT CCT TGG CAT CCT TAT CA	qChIP/qRT-PCR
EF1_F	CCA AGG GTG AAA GCA AGA AGA	qChIP/qRT-PCR
EF1_R	CTG GAG GTT TTG AGG CTG GTA T	qChIP/qRT-PCR
MYC2_A_F	CTCTTCCGATATCTCAACTTTATGG	qChIP
MYC2_A_R	GGCGTCGGAGTTGTTTCA	qChIP
miR156C_F	TTGCGTGCTCACTGCTCTAT	qChIP
miR156C_R	AGAGAAAGTGAGAGATGGGAACA	qChIP
AT1G21300-F	TGTACCAACAACGCTCCACT	qChIP
AT1G21300_R	TTTCCAGATAGCGAAGTTGTCTT	qChIP
AT1G47860_F	CCGCGTTTGCACCATTAT	qChIP
AT1G47860_R	CCATTGCCTACACGTACCG	qChIP
DOG1_F	TCTCGAGTGGATGAGTTTGC	qChIP
DOG1_R	TCTTCATCACCGTGAGAT CG	qChIP
ERF4_F	GTTTTCTTGCCCGGATCTC	qChIP
ERF4_R	CGTTAGGAAGCGTCCTTGG	qChIP
NAC19_F	TCTTCATCGGTCGGGTAAAATCGG	qChIP
NAC19_R	TCCAAGAAACTGACCCGTTAACGC	qChIP
JAZ1_B_F	GCAGAGAAGCAACAGCAACA	qCHIP
JAZ1_B_R	TCTCGAATAGCTAAATCGATACAAAG	qCHIP
JAZ9_A_F	GTCGAGAATAATGGAACATATTAAACC	qCHIP
JAZ9_A_R	GCAATAGGACGAACACAGTTATCA	qCHIP
JAZ9_B_F	TCTTCCTCTTCTTTAAATTGGATGTT	qCHIP
JAZ9_B_R	CAAACTCTCAAATTAACGTGTTTCTC	qCHIP
LOX3_A_F	CATCACAGAAAGGTCATCACTTG	qCHIP
LOX3_A_R	TTGATCGAGAACTGTGTTGACTG	qCHIP
LOX3_C_F	TTGGTACTCAGAATCAATCAACG	qCHIP
LOX3_C_R	GGTCGTCGACGGTTGATAA	qCHIP

Supplemental Table 7: List of primers.

The Arabidopsis hnRNP-Q Protein LIF2 and the PRC1 subunit LHP1 function in concert to regulate the transcription of stress-responsive genes

Anne Molitor, David latrasse, Matthias Zytnicki, Philippe Andrey, Nicole Houba-Hérin, Mélanie Hachet, Christophe Battail, Stefania Del Prete, Adriana Alberti, Hadi Quesneville and Valerie Gaudin

Plant Cell; originally published online August 5, 2016;
DOI 10.1105/tpc.16.00244